

The fate of the spin-1/2 Kondo effect in the presence of temperature gradients

Miguel A. Sierra,¹ Rosa López,¹ and David Sánchez¹

¹*Instituto de Física Interdisciplinar y Sistemas Complejos IFISC (UIB-CSIC), E-07122 Palma de Mallorca, Spain*

We consider a strongly interacting quantum dot connected to two leads held at quite different temperatures. Our aim is to study the behavior of the Kondo effect in the presence of large thermal biases. We use three different approaches, namely, a perturbation theory via the Kondo Hamiltonian, a slave-boson mean-field model of the Anderson model at large charging energies and a truncated equation-of-motion approach beyond the Hartree-Fock approximation. The two former approaches yield a suppression of the Kondo peak for thermal gradients above the Kondo temperature, showing a remarkably good agreement despite their different ranges of validity. The third approach allows us to analyze the full density of states within a wide range of energies. Additionally, we have investigated the quantum transport properties (electric current and thermocurrent) beyond linear response. In the voltage-driven case, we reproduce the split differential conductance due to the presence of different electrochemical potentials. In the thermocurrent, we observe a strongly nonlinear behavior as a function of the applied thermal gradient. Depending on the parameters, we can find nontrivial zeros in the temperature-driven current for finite values of the temperature bias. Importantly, these thermocurrent zeros yield direct access to the system's characteristic energy scales (Kondo temperature and charging energy).

PACS numbers: 73.23.-b, 73.50.Lw, 73.63.Kv, 73.50.Fq

I. INTRODUCTION

The Kondo effect is an intriguing subject in the condensed-matter community since it is a paradigmatic example of strong many-body physics [1]. Although this effect was firstly observed in metals with magnetic impurities, quantum dots (QDs) offer new possibilities for the manipulation of such many-body state owing to their tunability of the relevant parameters that control the physics of the problem. Since the discovery of the Kondo effect in semiconductor QD systems [2–6], interest has been spurred both experimentally and theoretically during the last decades. A prototypical setup showing Kondo physics consists of a QD (an artificial quantum impurity) connected to two reservoirs at a temperature T which is lower than a characteristic temperature scale dubbed Kondo temperature T_K . At such low temperature, the electric transport becomes highly correlated and the QD magnetic moment becomes screened by the electrons in the leads. A many-body singlet between the conducting and the localized electrons forms due to antiferromagnetic correlations originated from higher order spin-flip tunneling processes. At equilibrium, these correlations generate a sharp resonance in the local density of states around the Fermi energy ε_F whose width is of the order of $k_B T_K$ [7–9]. Importantly, the Kondo temperature depends highly on the system parameters, i.e., the position of the QD level relative to the Fermi energy, $\varepsilon_d - \varepsilon_F$, the charging energy of the electrons inside the dot U and the tunnel amplitude coupling to the reservoirs $\mathcal{V}_{\alpha k}$ (where α labels the lead connected to the dot and k the electronic wave number). When a voltage bias is applied between the left and right contacts, a current is driven through the QD. In this situation, the differential conductance shows a peak that mimics the Kondo resonance (zero bias anomaly or Abrikosov-Suhl resonance) [10]. For ap-

plied voltages of the order of $k_B T_K / e$, the peak splits and a strong dephasing destroys the Kondo resonance [11].

There exist very diverse theoretical approaches to deal with the Kondo effect that have been even applied to the theory of transport of more intricate QD arrangements like double or triple QDs [12, 13], spin-polarized QD systems [14, 15], hybrid superconducting-normal QD setups [16, 17], multiterminal QD systems [18, 19]. Further, depending on the range of temperatures and whether or not the system is driven out of equilibrium, some theoretical approximation schemes are more suitable than others. For instance, the equation of motion technique is fairly good to describe nonequilibrium Kondo physics for high and moderate temperatures (higher than T_K). This theoretical approach is able to explain the differential conductance splitting for voltages larger than $k_B T_K / e$. However, alternative models like the slave-boson mean field theory are more accurate for temperatures lower than T_K .

A relatively unexplored transport regime in systems exhibiting Kondo correlations is the effect of a temperature gradient applied between the electronic reservoirs. Indeed, the effect of increasing the background temperature in a Kondo quantum dot results in a destruction of the many-body singlet [1]. As a consequence, the system enters the Coulomb blockade regime where transport is only allowed when the additional charging energy U is supplied by externally gating the QD. Due to the Coulomb blockade effect, the differential conductance displays a Coulomb diamond structure as a function of the drain-source bias voltage and the dot level position. Inside the CB diamond, the conductance is strongly suppressed in contrast to the Kondo regime [6].

Temperature gradients can induce an electrical current (i.e., a thermocurrent) as well as voltage differences can induce a heat current. These cross phenomena are related in linear response due to Onsager reciprocity. The

thermoelectric current $I(\theta)$ gives the electrical current generated by a temperature bias θ in the absence of electrical gradients. Equivalently, a system under open circuit conditions ($I = 0$) creates a thermovoltage $V_{\text{th}}(\theta)$ in response to the thermal bias. Thermoelectric effects are essential for designing reliable devices that are able to convert waste heat into useful electric work [20]. Miniaturization progress has led to better performances [21]. For this reason, nanoscale conductors have attracted a lot of attention in a large variety of solid-state devices like QDs [22, 23], molecular bridges [24, 25], graphene layers [26, 27], quantum Hall junctions [28, 29], or quantum spin Hall systems [30, 31], just to mention a few. One of the first experiments probing the thermoelectrical transport in quantum systems was performed in a QD setup in the Coulomb blockade regime [32]. A sign change was observed in the thermovoltage V_{th} with the applied thermal bias. More recently, Svensson *et al.* [33] found analogous nonlinear effects in the thermovoltage properties of nanowire QDs. The latter experiments were theoretically addressed by two of us [34] in which the emergence of highly nonlinear effects in the thermocurrent I_{th} and thermovoltage V_{th} nicely agreed with the experimental results. A Hartree-Fock scheme using nonequilibrium Green's functions within the equation-of-motion formalism was employed to model the thermoelectric transport in the Coulomb blockade regime. The origin of nonlinear thermocurrents and thermovoltages is related to a change in the direction of the electrical flow due to the different QD resonance contributions. As a consequence, the differential thermoelectric conductance plots present a butterfly shape. Later on, Svilans *et al.* [35] reported similar experimental findings.

The purpose of this work is to go beyond the Coulomb blockade regime and to thoroughly investigate the nonlinear thermoelectric properties of quantum dots in the Kondo regime. Our first aim is to determine the fate of the Kondo effect upon application of a thermal gradient. In particular, we will discuss how the position of the Kondo peak and the Kondo temperature get modified due to thermal biases. We address this problem by employing different theoretical approaches: nonequilibrium Green's function formalism (NEGF) with higher-order equation of motion (EOM), slave-boson mean-field theory (SBMFT) and perturbative approach. These schemes encompass the whole range of temperatures, well below the Kondo temperature and for temperatures of the order or higher than T_K . We compare the different approximations and study their range of validity. Importantly, we predict for the first time that the Kondo resonance is destroyed when the thermal bias θ is sufficiently strong. This result is obtained using both perturbative and SBMFT approaches. Further, we are able to give a fully analytical expression for the Kondo quench within perturbation theory. Our second aim is to analyze the transport properties of the system driven out of the equilibrium with both voltage and thermal biases and to examine the current behavior for arbitrary values

of θ . Our main finding in this case is a strong nonlinear behavior in the EOM current characteristics due to the existence of the Kondo resonance and the single-particle peaks. This is a relevant result because it would allow to experimentally measure the system's energy scales from the nontrivial zeros of the current.

Despite the fact that nonlinear thermoelectrics [36] in Kondo-correlated systems is quite a new topic, there is already a number of interesting results in the last years. Most of them are focused on the study of the Seebeck coefficient $S = V_{\text{th}}/\theta$ employing a large variety of methods: nonperturbative resonant tunneling approximation [37], second-order perturbation theory for the onsite Coulomb interaction [38], slave-boson non-crossing approximation (NCA) [39], generalized Keldysh-based NCA [40], nonequilibrium Green's functions beyond Hartree-Fock [41], quantum [42] and auxiliary [43] master equation approaches and dual fermions renormalized perturbation theory (RPT) [44]. In the linear regime, experimental evidence of the influence of the Kondo effect in the thermopower of a QD was reported in Ref. [45]. Thermopower and strong correlations are the subject of Refs. [46, 47]. The Seebeck coefficient of an Aharonov-Bohm interferometer with an embedded QD shows modulated sign and magnitude [48]. When coupled to ferromagnetic leads, the quantum dot exhibits spin-dependent thermopowers [49, 50]. Double quantum dots supporting molecular states are believed to display enhanced thermoelectric power [51]. The spin Seebeck coefficient, which measures the spin current generated in response to a thermal gradient, shows interesting features when many-body interactions are taken into account [52–54]. It turns out that the thermopower is a highly sensitive probe of correlations in QD systems with SU(4) Kondo symmetry [55]. Kondo physics is able to boost the power output and efficiency [40, 56]. The effect of spin-orbit coupling of the Rashba type is treated in Ref. [57]. Finally, we briefly mention additional interesting topics where thermoelectrics in Kondo artificial impurities play a significant role: relaxation dynamics [58], orbital degrees of freedom [59, 60], universal ac thermopower [61], hybrid devices connected to ferromagnetic and superconducting leads [62], assisted hopping [63] and different configurations such as parallel [64] or side coupled double QDs [65].

Our paper is organized as follows. In Sec. II we describe our model Hamiltonian. We then present in Sec. III a perturbative analysis for the case where a thermal gradient is applied across a two-terminal quantum dot. In Sec. IV we employ the slave-boson mean-field theory and investigate how the width and position of the Kondo peak are modified under voltage and thermal bias. We compute the thermoelectric current when Kondo correlations are present. We treat the high and moderate temperature regimes by using the equation-of-motion approach in Sec. V. We consider the limit of large Coulomb repulsion and analyze the nonlinear transport when large voltages and thermal biases are considered.

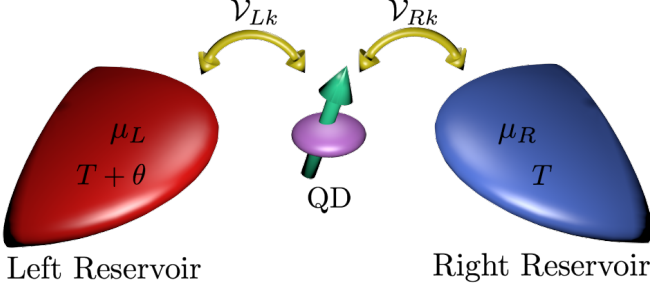


FIG. 1. (Color online) Sketch of the quantum dot system under the influence of a voltage ($\mu_L - \mu_R$) and temperature gradient (θ) applied between the two reservoirs. The system consists of two reservoirs (left L and right R) connected through tunnel barriers (with tunneling amplitudes $\mathcal{V}_{\alpha k}$) to an interacting quantum dot acting as an artificial quantum impurity (green arrow).

We summarize our main findings in Sec. VI.

II. MODEL HAMILTONIAN

The setup under consideration is described by the single-impurity Anderson Hamiltonian [66]. It describes the localized quantum dot level connected by tunneling barriers to two electronic reservoirs denoted with $\alpha = \{L, R\}$. Each reservoir has an electrochemical potential $\mu_\alpha = \varepsilon_F + eV_\alpha$ and a temperature $T_\alpha = T + \theta_\alpha$ as shown in Fig. 1. We hereafter consider $\varepsilon_F = 0$, $V_L = -V_R = V/2$, $\theta_L = \theta$, $\theta_R = 0$.

The total Hamiltonian is the sum of the following contributions:

$$\mathcal{H} = \mathcal{H}_{\text{leads}} + \mathcal{H}_{\text{dot}} + \mathcal{H}_{\text{tun}}, \quad (1)$$

The reservoir Hamiltonian reads

$$\mathcal{H}_{\text{leads}} = \sum_{\alpha k \sigma} \varepsilon_{\alpha k} C_{\alpha k \sigma}^\dagger C_{\alpha k \sigma}, \quad (2)$$

where $\varepsilon_{\alpha k}$ is the energy dispersion relation for the α -lead. Here, $C_{\alpha k \sigma}^\dagger$ ($C_{\alpha k \sigma}$) corresponds to the creation (annihilation) operator of an electron in the α -lead with wavenumber k and spin $\sigma = \{\uparrow, \downarrow\}$. The quantum dot system reads

$$\mathcal{H}_{\text{dot}} = \sum_{\sigma} \varepsilon_d d_{\sigma}^\dagger d_{\sigma} + U d_{\uparrow}^\dagger d_{\downarrow}^\dagger d_{\downarrow} d_{\uparrow}, \quad (3)$$

where the localized energy level is ε_d and the charging energy is U . The tunnel Hamiltonian is represented as

$$\mathcal{H}_{\text{tun}} = \sum_{\alpha k \sigma} \mathcal{V}_{\alpha k} C_{\alpha k \sigma}^\dagger d_{\sigma} + \text{H.c.} \quad (4)$$

Here, $\mathcal{V}_{\alpha k}$ are the tunneling amplitudes. We neglect its dependence on the spin quantum number, which is relevant for ferromagnetic electrodes [14, 15] or magnetic fields [67–69].

III. PERTURBATIVE APPROACH

For the perturbative analysis, it is advantageous to resort to the Kondo Hamiltonian by means of a Schrieffer-Wolff transformation [1]. We remark that this Hamiltonian equivalence is only valid for the deep Kondo regime. Then, the Kondo Hamiltonian is $\mathcal{H}_K = \mathcal{H}_0 + \mathcal{H}_1$, where

$$\mathcal{H}_0 = \sum_{\alpha k \sigma} \varepsilon_{\alpha k \sigma} C_{\alpha k \sigma}^\dagger C_{\alpha k \sigma}, \quad (5)$$

and

$$\mathcal{H}_1 = \sum_{\alpha k \sigma \beta q s} \mathcal{J}_{\alpha \beta}(t) x_{\sigma s} C_{\alpha k \sigma}^\dagger C_{\beta q s}, \quad (6)$$

where $x_{\sigma s} = \delta_{\sigma s}/4 + \hat{S}_l s_{\sigma s}^l$ is defined in terms of the quantum dot (S_l , $l = x, y, z$) and lead (s_l) spin operators, respectively. The Kondo coupling,

$$\mathcal{J}_{\alpha \beta}(t) = \mathcal{J}_{\alpha \beta}^{(0)} \exp\left(-\frac{ie}{\hbar} [V_\alpha - V_\beta] t\right), \quad (7)$$

depends on the voltage difference between the two reservoirs with $\mathcal{J}_{\alpha \beta}^{(0)} = -\mathcal{V}_\alpha \mathcal{V}_\beta U / [\varepsilon_d (U + \varepsilon_d)]$. We calculate the electrical conductance in perturbation theory up to third order in the Kondo coupling (\mathcal{H}_1) [70, 71]. To do so, we first consider the expected value of the current operator,

$$I = \langle \mathcal{S}(-\infty, 0) \hat{I}(0) \mathcal{S}(-\infty, 0) \rangle, \quad (8)$$

with $\mathcal{S}(-\infty, 0)$ the S-matrix given in terms of the perturbation \mathcal{H}_1

$$\mathcal{S}(-\infty, 0) = \hat{T} \int_{-\infty}^0 \mathcal{H}_1(\tau) d\tau. \quad (9)$$

Here, \hat{T} is the time-ordered operator. The explicit expression for the α -current operator stems from the time derivative of the occupation number operator at lead α , $\hat{I}_\alpha = -e \sum_{k \sigma} \partial_t (C_{\alpha k \sigma}^\dagger C_{\alpha k \sigma})$. After a few algebraic manipulations we arrive at

$$\hat{I}(t) = \frac{ie}{\hbar} \sum_{k q \sigma s} (\mathcal{J}_{LR}(t) x_{\sigma s} C_{L k \sigma}^\dagger C_{R q s} - \text{H.c.}) \quad (10)$$

The calculation of Eq. (8) up to third order in the Kondo coupling by using Eq. (9) and Eq. (10) requires a lengthy algebra that is discussed in detail in App. A. After calculating the current expectation value, it is straightforward to obtain the expression for the electrical conductance $G \equiv dI/dV$ with $V = V_L - V_R$. We find

$$G = -\frac{3e^2 \pi}{4\hbar} \nu^2 [\mathcal{J}_{LR}^{(0)}]^2 \left(1 - \frac{\nu}{2} (\mathcal{J}_{LL}^{(0)} + \mathcal{J}_{RR}^{(0)}) \ln \left| \frac{k_B^2 T_L T_R}{D_0^2} \right| \right) - \frac{e^2 \pi}{4\hbar} \nu^2 [\mathcal{J}_{LR}^{(0)}]^2. \quad (11)$$

Here, $D_0 = \sqrt{-\varepsilon_d (U + \varepsilon_d)}$ is the effective bandwidth, and ν is the density of states of the leads, which we assume

flat (wide band limit). The conductance G has two contributions: the exchange cotunneling and the regular cotunneling terms [first and second lines in Eq. (11), respectively]. Notice that the logarithmic divergence contains the product of the reservoir temperatures. If we do not consider thermal gradients, our expression reduces to the conductance obtained in Ref. [71]. The Kondo temperature is defined as the temperature at which the second order contribution in Eq. (11) dominates over the first term. When there is neither thermal nor voltage biases applied to our system, we recover the usual Kondo temperature at equilibrium [72]

$$k_B T_{K0} = D_0 \exp \left[\frac{\pi \varepsilon_d (U + \varepsilon_d)}{U \Gamma} \right]. \quad (12)$$

Here $\Gamma = \Gamma_L + \Gamma_R$ is the total level broadening due to tunneling, with $\Gamma_\alpha(\omega) = \pi \nu |\mathcal{V}_\alpha(\omega)|^2$, which we take as a constant parameter.

We now substitute $T_L = T + \theta$ and $T_R = T$ in Eq. (11). Therefore, the Kondo temperature reads

$$T_K(\theta) = \sqrt{\left(\frac{\theta}{2}\right)^2 + T_{K0}^2} - \frac{\theta}{2}. \quad (13)$$

This is a central result of our paper. It yields the Kondo temperature as a function of the thermal gradient across a QD. Equation (13) dictates that T_K decreases as θ increases and eventually vanishes for very high values of the temperature bias. Our perturbative approach thus shows that a large thermal gradient kills the Kondo effect. However, Kondo correlations can survive for small values of θ . These findings are illustrated in Fig. 2 (see solid blue curve). Here, the normalized Kondo temperature T_K/T_{K0} is displayed as a function of θ . We plot the Kondo temperature in a logarithmic scale for clarity. We observe that for small θ values the Kondo temperature stays roughly constant (Kondo regime) until θ becomes close to the equilibrium Kondo temperature, where T_K drops quickly (scaling region) and then vanishes monotonically (Kondo quench).

IV. SLAVE-BOSON THEORY

The perturbative approach presented above is only suitable for background temperatures higher than T_K because at low temperatures the logarithmic dependence shown in Eq. (11) dominates and diverges. The previous analysis is, by nature, a perturbative method and breaks down at low temperatures. In order to extend our analysis toward the low temperature regime, we now analyze the same setup (a quantum impurity in the presence of large temperature biases). Several models are able to explain the Fermi liquid regime i.e. renormalized perturbation theory [73, 74]. However, we choose to use the slave-boson mean-field theory (SBMFT), which is also known to give accurate results in the limit $T \rightarrow 0$.

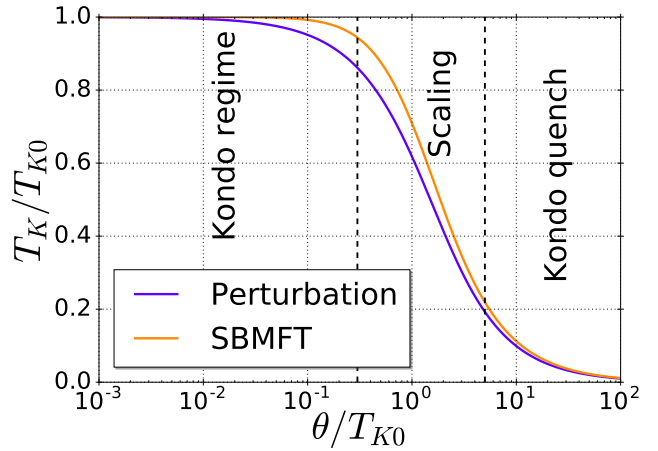


FIG. 2. (Color online). Normalized Kondo temperature T_K/T_{K0} as a function of the thermal gradient θ/T_{K0} applied to a two-terminal quantum dot when $T_L = T + \theta$, and $T_R = T$. Blue line corresponds to the perturbative analysis result whereas orange line shows the Kondo temperature derived from the slave boson mean-field theory. Here, $T_{K0} = T_K(0)$ is defined as the Kondo temperature at equilibrium [see Eqs. (12) and (22)].

Let us consider the Anderson Hamiltonian description [Eq. (1)] in the limit $U \rightarrow \infty$. This limit gives the correct low temperature behavior for the deep Kondo regime [75]. In the slave-boson formalism [1] the dot operator $d_\sigma = b^\dagger f_\sigma$ is replaced by the product of a pseudofermion operator f_σ and a boson field operator b^\dagger . When an electron with spin σ is annihilated in the dot a vacuum state is created, which is represented by the boson creation operator b^\dagger and the pseudofermion annihilation operator f_σ . Then, the tunneling Hamiltonian becomes

$$\mathcal{H}_{\text{tun}} = \sum_{\alpha k \sigma} \mathcal{V}_{\alpha k} C_{\alpha k \sigma}^\dagger b^\dagger f_\sigma + \text{H.c.} \quad (14)$$

To properly carry out the perturbation theory using \mathcal{H}_{tun} as a perturbation term, we need to rescale the tunneling amplitudes as $\mathcal{V}_{\alpha k} \rightarrow \tilde{\mathcal{V}}_{\alpha k} \equiv \mathcal{V}_{\alpha k}/\sqrt{N}$ with N representing the angular momentum degeneracy. The perturbation theory is done in the parameter $1/N$. Strictly when $N \rightarrow \infty$ the perturbation theory leads to exact results [75]. We impose the condition $U \rightarrow \infty$ by adding a Lagrange multiplier λ to the Hamiltonian as

$$\mathcal{H}_{\text{Lag}} = \lambda \left(b^\dagger b + \sum_\sigma f_\sigma^\dagger f_\sigma - 1 \right). \quad (15)$$

This term ensures that the Hilbert space does not contain the double occupancy dot state.

Next, we consider the mean-field solution of the Hamiltonian. This corresponds to the lowest order in the large- N expansion. In this approximation, the boson operator is replaced by its mean value $\langle b \rangle = \bar{b}$, \bar{b} being a c -number. This way, charge fluctuations are completely screened out. The assumption is valid as long as $T < T_K$ and

the dot level lies within the Kondo regime (Fermi liquid fixed point). Our goal is then to derive the mean-field equations for both the expectation value of b and the Lagrange multiplier. We first determine the equation of motion for the boson operator in the stationary limit,

$$\sum_{\alpha k \sigma} \tilde{V}_{\alpha k} G_{f\sigma, \alpha k \sigma}^<(t, t) = -iN\lambda |\tilde{b}|^2, \quad (16)$$

where $G_{f\sigma, \alpha k \sigma}^<(t, t') = -(i/\hbar) \langle C_{\alpha k \sigma}^\dagger(t') f_\sigma(t) \rangle$ is the lesser Green's function of the tunneling process [76]. The second mean-field equation is directly the equation for the Lagrange multiplier that imposes the closure relation for the restricted Hilbert space [Eq. (15)] in terms of the mean-field value of the boson operator

$$\sum_{\sigma} G_{f\sigma, f\sigma}^<(t, t) = i(1 - N|\tilde{b}|^2), \quad (17)$$

where $G_{f\sigma, f\sigma}^<(t, t') = -(i/\hbar) \langle f_{\alpha k \sigma}^\dagger(t') f_\sigma(t) \rangle$ is the dot pseudofermion lesser Green's function. The two nonlinear equations, Eqs. (16) and (17), need to be solved self-consistently. By combining Eqs. (16) and (17) in a single complex equation and resorting to the Fourier space one gets

$$\frac{2}{\pi} \int_{-D}^D d\omega \frac{\mathcal{F}(\omega)}{\omega - \tilde{\varepsilon}_d + i\tilde{\Gamma}} = (\varepsilon_d - \tilde{\varepsilon}_d) \frac{N}{\Gamma} - i \left(1 - N \frac{\tilde{\Gamma}}{\Gamma} \right) \quad (18)$$

where $\tilde{\varepsilon}_d = \varepsilon_d + \lambda$ is the renormalized dot level position due to the Kondo correlations and $\mathcal{F}(\omega)$ is a nonequilibrium distribution function [77]

$$\mathcal{F}(\omega) = \sum_{\alpha} \frac{\Gamma_{\alpha} f_{\alpha}(\omega)}{\Gamma}. \quad (19)$$

Here, $f_{\alpha}(\omega) = 1/[1 + \exp\{(\omega - \mu_{\alpha})/(k_B T_{\alpha})\}]$ is the Fermi-Dirac function of lead α . Once the two mean-field parameters are determined, we are in a position to compute the QD spectral function

$$\rho_{d\sigma}(\omega) = -\frac{|\tilde{b}|^2}{\pi} \text{Im}[G_{f\sigma, f\sigma}^r(\omega)], \quad (20)$$

where $G_{f\sigma, f\sigma}^r(t, t') = -\frac{i}{\hbar} \theta(t - t') \langle [f_{\sigma}^\dagger(t'), f_{\sigma}(t)]_+ \rangle$ is the dot retarded Green's function in terms of $[\dots]_+$, the anticommutator of two operators. Calculating the equation of motion for this Green's function, we find a closed system of equations that gives

$$\rho_{d\sigma}(\omega) = \frac{|\tilde{b}|^2}{\pi} \frac{\tilde{\Gamma}}{(\omega - \tilde{\varepsilon}_d)^2 + \tilde{\Gamma}^2}. \quad (21)$$

Usually the Kondo resonance is pinned at the Fermi energy. Then, $\tilde{\varepsilon}_d \approx \varepsilon_F$, leading to the Kondo resonance. Similarly, this resonance has a width $\tilde{\Gamma} = |\tilde{b}|^2 \Gamma$ renormalized by Kondo correlations and which can be identified with the Kondo temperature. We remark that Eq. (21) obeys the Friedel sum rule, $\pi \Gamma \rho_{d\sigma}(\tilde{\varepsilon}_d) = 1$, even though the energy integration is not able to give the full occupation since SBMFT does not capture the single-particle peaks. SBMFT only describes the Kondo peak properly, which nevertheless suffices for our purpose of analyzing the Kondo temperature, as we next discuss.

A. Kondo Temperature

Let us determine how small electrical and thermal biases modify the Kondo resonance within SBMFT. To obtain analytical results we consider $|\varepsilon_{d\sigma}| \gg \tilde{\varepsilon}_{d\sigma}$ (deep Kondo regime) together with $|\tilde{b}|^2 \ll 1$ (Fermi liquid). At equilibrium and for $T = 0$ the Kondo temperature $k_B T_K = |\tilde{b}|^2 \Gamma$ takes the form

$$\tilde{\Gamma} = k_B T_K = D e^{-\pi|\varepsilon_d|/\Gamma}, \quad (22)$$

where D is the lead bandwidth. In the voltage-driven case, but still $T = 0$, the nonequilibrium distribution function appearing in Eq. (18) plays a fundamental role when the Kondo temperature is computed as a function of the voltage bias. In such case, the distribution function becomes a doubly stepped function depending on the voltage of the leads. Hence, one arrives at the following expressions:

$$\tilde{\Gamma} \tilde{\varepsilon}_d = 0, \quad (23)$$

$$\tilde{\varepsilon}_d^2 - \left(\frac{eV}{2} \right)^2 - \tilde{\Gamma}^2 = -k_B^2 T_K^2. \quad (24)$$

Remarkably, when eV approaches $2k_B T_K$ the Kondo temperature drops to zero whereas $\tilde{\varepsilon}_d \approx 0$ due to the fact that $\tilde{b} \rightarrow 0$ and $\lambda = -\varepsilon_{d\sigma}$. Then, at exactly $eV = 2k_B T_K$ a phase transition occurs and the renormalized dot level position undergoes a bifurcation. Such a bifurcation indicates that the Kondo resonance splits due to the presence of the electrical bias. This result agrees with the calculations made in Refs. [78, 79] and the experimental result shown in Ref. [10]. We note that SBMFT is valid for voltages smaller than $2k_B T_K$ since the predicted phase transition is in reality a crossover. However, the general behavior is correct and suffices for our purposes.

We present in Fig. 3 our numerical results for Eq. (18) in the voltage-driven case and $T = 0$. We observe that the numerical result fits nicely with the analytical result found in Eq. (24) specially for the deep Kondo regime (see the case for $\varepsilon_d = -3.5\Gamma$). The phase transition occurs when $eV = 2k_B T_K$, at which point the splitting of the Kondo resonance takes place [Fig. 3(a)]. When the dot level approaches towards the mixed-valence regime ($\varepsilon_d \simeq -\Gamma$), charge fluctuations become important and the phase transition occurs at much lower voltage bias values. As expected, the Kondo resonance becomes narrower as voltage grows [Fig. 3(b)].

For the temperature-driven case an analytical treatment can be also performed, leading to the result

$$\sum_{\alpha} \frac{\Gamma_{\alpha}}{\Gamma} \left[\log \left| \frac{2\pi k_B T_{\alpha}}{D} \right| + \psi \left(\frac{1}{2} + \frac{i\tilde{\varepsilon}_d + \tilde{\Gamma}}{2\pi k_B T_{\alpha}} \right) \right] = \frac{\pi N \varepsilon_d}{2\Gamma}, \quad (25)$$

where $\psi(x)$ denotes the digamma function. By expanding the digamma function around $T = 0$ we find the leading order contribution for the Kondo temperature within a temperature gradient expansion. This amounts to considering a Sommerfeld expansion in the integral of

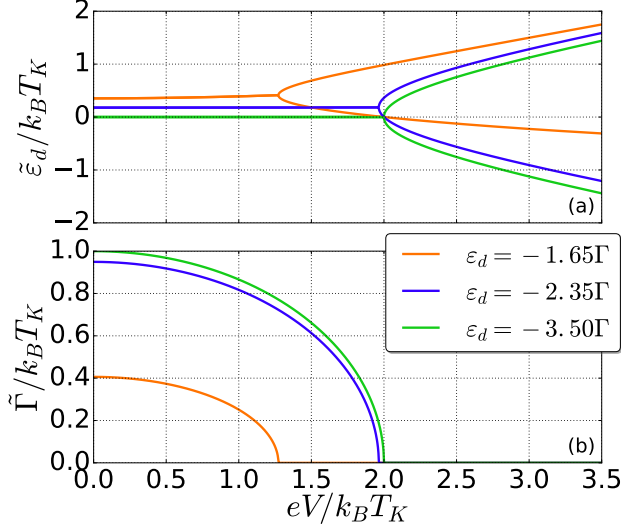


FIG. 3. (Color online). Position of the SBMFT (a) renormalized energy level $\tilde{\epsilon}_d$ and (b) width $\tilde{\Gamma}$ as a function of the applied voltage for different dot level positions. The case $\epsilon_d = -3.5\Gamma$ agrees with the analytical result given by Eq. (24). Parameters: $D = 100\Gamma$, $k_B T \approx 0$ and $\Gamma_L = \Gamma_R = \Gamma/2$.

Eq. (18). However, we need to calculate the second order term to get a thermal gradient dependence of T_K ,

$$\tilde{\epsilon}_d = 0, \quad (26)$$

$$\tilde{\Gamma} = k_B T_K e^{-\frac{\pi^2}{12} \frac{T_L^2 + T_R^2}{T_K^2}}. \quad (27)$$

The solution of the mean-field equations demonstrates that a thermal gradient, in contrast to a voltage bias, does not cause any Kondo splitting but merely renormalizes the Kondo resonance width. This renormalization is a decreasing function of the thermal bias θ . We stress that this approximation is only valid for very low temperatures $T_L, T_R \ll 1$ for which SBMFT can be applied (see the inset of Fig. 4). Still, we arrive at the same conclusion as in the perturbation scheme of the previous section: a strong thermal bias destroys the Kondo effect. The narrowing of the Abrikosov-Suhl resonance is the smoking gun of this quenching.

Our numerical results for $\theta > 0$ are displayed in Fig. 4. Importantly, our analytical results agree well with the numerical curves provided we are in the deep Kondo regime ($\epsilon_d = -3.5\Gamma$). Thus, as long as ϵ_d enters the mixed-valence regime, we find departures from the analytical calculation, as expected. We observe three distinct regions for the T_K curves depending on the θ value. Thus, for a low temperature bias $\theta \ll 0.1T_K$ the renormalized parameters remain almost unaffected. With increasing θ as $0.1T_K < \theta < 10T_K$ the Kondo temperature decays exponentially and eventually drops to zero.

Surprisingly, the agreement between our perturbative analysis and the SBMFT result illustrated in Fig. 2 is quite good. In both cases, we find a decrease of the en-

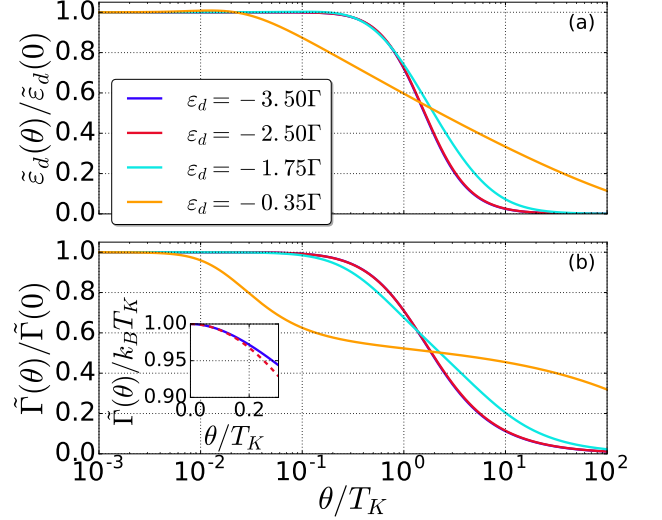


FIG. 4. (Color online). (a) Renormalized dot gate position $\tilde{\epsilon}_d$ and (b) width $\tilde{\Gamma}$ as a function of the thermal bias θ for different ϵ_d values within SBMFT. Inset: resonance width versus the thermal bias from a numerical calculation (solid line) and from the analytical expression given by Eq. (27) (dashed line) for $\epsilon_d = -3.5\Gamma$. Parameters: $D = 100\Gamma$, $k_B T \approx 0$, and $\Gamma_L = \Gamma_R = \Gamma/2$.

ergy binding of the many-body Kondo singlet as a function of the thermal bias. Notice that such agreement between both approaches holds even when the considered θ values are away from the range of validity for the SBMFT (θ small compared to T_{K0}) and the perturbative analysis (θ large compared to T_{K0}), which further supports the robustness of our main conclusion.

Let us now consider cross thermal and electrical effects arising when both voltage and temperature biases act at the same time. In Fig. 5 we show the renormalized parameters versus θ for different values of eV/T_K . Remarkably enough, in Fig. 5(b) we discover the occurrence of a maximum when $\theta \approx T_K$ for dot level positions near the mixed-valence regime. Similarly to the purely thermal case (i.e., $V = 0$), we observe three different behaviors for $\tilde{\Gamma}/T_K$ with increasing θ , namely, when $\theta < 0.1T_K$ the Kondo width is almost unmodified, then it drops quickly towards zero when $T_K < \theta < 2T_K$. However, when V is nonzero a nonmonotonic behavior yields a local maximum. The peak position depends on the applied voltage and shifts towards higher θ values as V grows. Our results suggest that the Kondo resonance becomes reinforced in the presence of a thermal gradient if a voltage bias is also present. This is an unexpected effect because a nonequilibrium field usually destroys a given coherent state (a notable exception is the laser). Here, electric and thermal gradients alone quench the Kondo effect but the synergistic combination between the two can generate a Kondo reentry. We further clarify this finding by plotting the resonance position [Fig. 6(a)] and width [Fig. 6(b)]

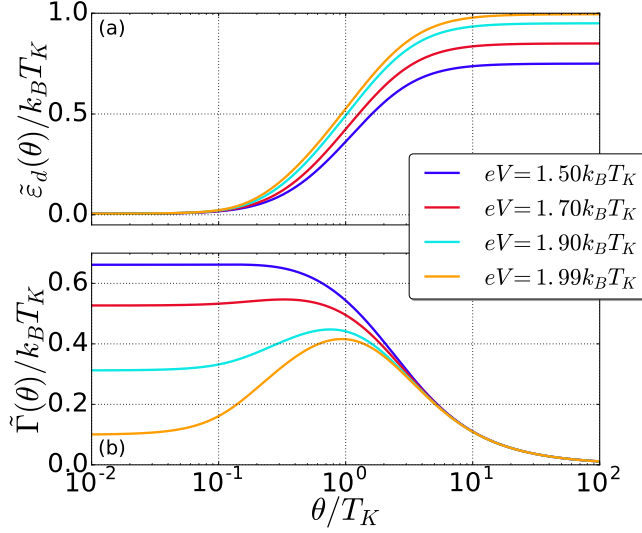


FIG. 5. (Color online). (a) Position of the renormalized energy level $\tilde{\varepsilon}_d$ and (b) width $\tilde{\Gamma}$ as a function of the thermal bias for different eV . Parameters: $\varepsilon_d = -3.5\Gamma$, $D = 100\Gamma$, $k_B T \approx 0$ and $\Gamma_L = \Gamma_R = \Gamma/2$

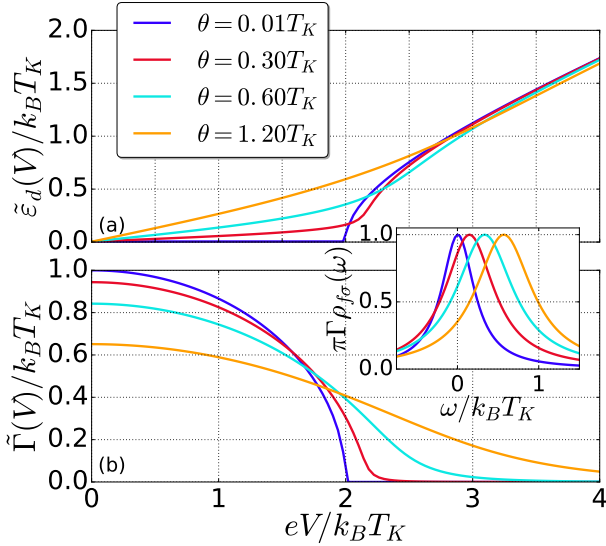


FIG. 6. (Color online). (a) Position of the renormalized energy level $\tilde{\varepsilon}_d$ and (b) width $\tilde{\Gamma}$ as a function of the thermal bias for different $k_B \theta$. Inset: Local density of states for different values of the thermal bias and for $eV = 1.94 k_B T_K$. Parameters: $\varepsilon_d = -3.5\Gamma$, $D = 100\Gamma$, $k_B T \approx 0$ and $\Gamma_L = \Gamma_R = \Gamma/2$

as a function of voltage for different values of θ . The key point is to notice that, when the width decreases for small V , at large voltages the action of θ is to smear out the width decrease, extending the range of nonzero values of $\tilde{\Gamma}$ beyond the original $\theta = 0$ interval. As a consequence, increasing both voltage and temperature biases helps the Kondo resonance survive out of equilibrium.

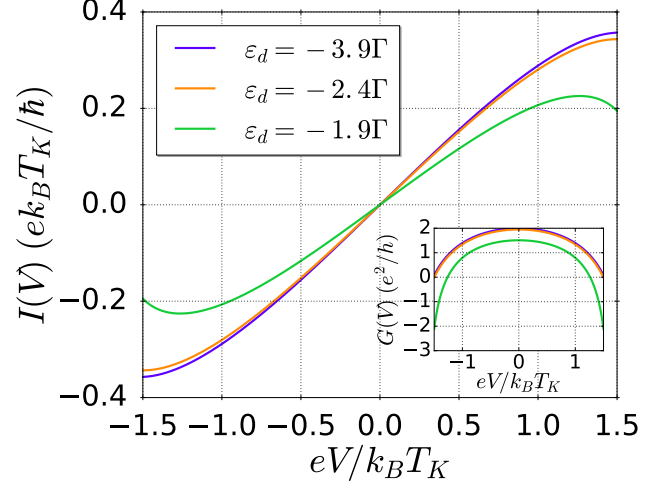


FIG. 7. (Color online). Current-voltage characteristics of a single level quantum dot in the Kondo regime using slave-boson mean-field theory for different values of the gate voltage (level position). Inset: Differential conductance of the quantum dot as a function of the applied voltage. Parameters: $D = 100\Gamma$, $k_B T \approx 0$, and $\Gamma_L = \Gamma_R = \Gamma/2$

B. Transport properties

Once the renormalized parameters are determined for a thermoelectric configuration the electrical current can be readily computed. We recall that the current is defined as the time derivative of the occupation of one of the leads $I_{\alpha} = -e \sum_{k\sigma} \partial_t \langle C_{\alpha k\sigma}^{\dagger} C_{\alpha k\sigma} \rangle$. Using the current conservation condition for steady-state currents ($I \equiv I_L = -I_R$) and considering the wide band limit, the current reads

$$I = -\frac{e}{\pi \hbar} \int_{-\infty}^{\infty} d\omega \sum_{\sigma} \frac{\Gamma_L \Gamma_R}{\Gamma} \text{Im}[G_{\sigma,\sigma}^r(\omega)] (f_L(\omega) - f_R(\omega)), \quad (28)$$

where $G_{\sigma,\sigma}^r(t, t') = -\frac{i}{\hbar} \theta(t-t') \langle [d_{\sigma}^{\dagger}(t'), d_{\sigma}(t)]_+ \rangle$ is the QD retarded Green's function. Following the same procedure as above and performing the integration, one arrives at

$$I = I_0 \text{Im} \left[\psi \left(\frac{1}{2} + \frac{i(\tilde{\varepsilon}_d - \mu_R) + \tilde{\Gamma}}{2\pi k_B T_R} \right) - \psi \left(\frac{1}{2} + \frac{i(\tilde{\varepsilon}_d - \mu_L) + \tilde{\Gamma}}{2\pi k_B T_L} \right) \right], \quad (29)$$

where $I_0 = (4e\Gamma_L\Gamma_R)/(\hbar\Gamma)$. In Fig. 7, the $I - V$ characteristic curves are shown for different dot gate positions. At very low voltages the current is linear with the bias voltage as expected, then by increasing eV the current reaches its maximum value and the dot becomes fully transparent. From the $I - V$ curve it is easy to obtain the differential conductance which at zero bias reaches its maximum value (see the inset of Fig. 7).

In Fig. 8 we show the results for the electrical current when a temperature shift is applied for different dot gate positions. We observe that the thermocurrent attains higher values for dot level positions that are away from the deep Kondo regime, a regime in which electron-

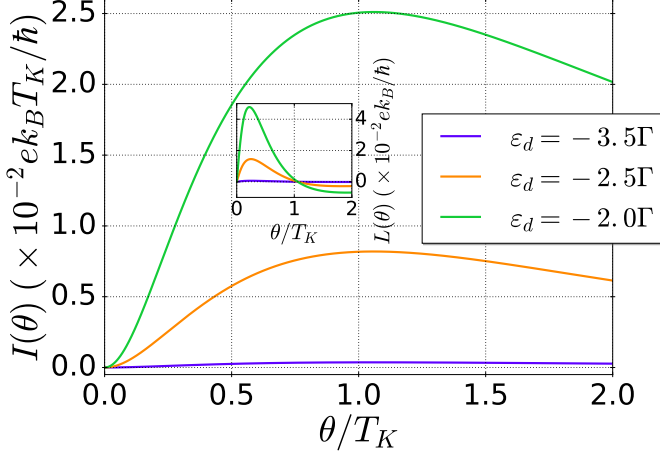


FIG. 8. (Color online). Thermocurrent as a function the thermal gradient θ of a single level quantum dot in the Kondo regime using slave-boson mean-field theory for different values of the dot gate position. Inset: Thermoelectric conductance as a function of the thermal bias for the same dot gate positions. Parameters: $D = 100\Gamma$, $k_B T \approx 0$ and $\Gamma_L = \Gamma_R = \Gamma/2$

hole symmetry breaking is more prominent. If we express the current as $I \simeq L_1\theta + L_2\theta^2$, particle-hole symmetry is responsible for vanishing thermoelectric conductance in linear response ($L_1 \simeq 0$) since the transmission probability does not change significantly with the temperature bias. Then, the leading order at low thermal shifts is given by

$$L_2 = \frac{4\pi^2 e k_B^2}{3h} \tilde{\Gamma}_L \tilde{\Gamma}_R \frac{\tilde{\varepsilon}_d}{\tilde{\varepsilon}_d^2 + \tilde{\Gamma}^2}. \quad (30)$$

Remarkably, the sign of L_2 in Eq. (30) depends on the renormalized dot level position. Thus we observe that deep in the Kondo regime ($\tilde{\varepsilon}_d \simeq 0$) the thermoelectric current is vanishingly small, even beyond linear response. This is better seen in the inset in Fig. 8, which depicts the nonlinear thermoelectric conductance $L = dI/d\theta$. The purple curve corresponds to the Kondo limit, which deviates little from the zero value. When the dot level shifts to higher energies closer to the Fermi energy the thermoelectric conductance behavior is more interesting. For instance, it shows a maximum value for small values of θ and then changes its sign. The maximal L grows as the dot gate position enters the mixed-valence regime due to the lack of electron-hole symmetry. The change of sign occurs at thermal biases of the order of the Kondo temperature because for larger values of θ the thermocurrent starts to decrease due to the quench of the Kondo effect (main panel of Fig. 8).

V. EQUATION-OF-MOTION TECHNIQUE

In this section, we address the thermoelectric transport in the Anderson model for the case of moderate temperatures. In Sec. III, we have employed the perturbative analysis, which is also suitable for high temperatures, to derive the Kondo temperature $T_K(\theta)$ for a finite temperature shift. However, perturbation theory does not allow us to access dynamical quantities like the local density of states. Therefore, in this section we propose an equation-of-motion (EOM) scheme that permits to study the role of single-particle peaks in addition to the Kondo resonance. In particular, we will be able to study the impact of the different resonances in the nonlinear transport regime. The EOM method aims at obtaining the retarded Green's function of the dot $G_{\sigma,\sigma}^r$ within the Keldysh formalism [76, 80, 81]. We find (the full calculation of $G_{\sigma,\sigma}^r$ is included in App. B):

$$G_{\sigma,\sigma}^r(\omega) = \frac{1 - \langle \tilde{n}_{\bar{\sigma}} \rangle}{\omega - \varepsilon_d - \Sigma_0 + U \Sigma_1 / [\omega - \varepsilon_d - U - \Sigma_0 - \Sigma_3]} + \frac{\langle \tilde{n}_{\bar{\sigma}} \rangle}{\omega - \varepsilon_d - \Sigma_0 - U - U \Sigma_2 / [\omega - \varepsilon_d - \Sigma_0 - \Sigma_3]}, \quad (31)$$

where $\bar{\sigma}$ denotes the spin opposite to σ and

$$\Sigma_0 = \sum_{\alpha k} \frac{|\mathcal{V}_{\alpha k}|^2}{\omega - \varepsilon_{\alpha k}}, \quad (32)$$

$$\Sigma_1 = \sum_{\alpha k} \frac{\mathcal{V}_{\alpha k}^*}{\omega - \varepsilon_{\alpha k}} \left[\sum_{\beta q} (\mathcal{V}_{\beta q} \langle C_{\beta q \bar{\sigma}}^\dagger C_{\alpha k \bar{\sigma}} \rangle - \Sigma_0 \langle d_{\bar{\sigma}}^\dagger C_{\alpha k \bar{\sigma}} \rangle) \right] + \sum_{\alpha k} \frac{\mathcal{V}_{\alpha k}}{-\omega_1 + \varepsilon_{\alpha k}} \left[\sum_{\beta q} (\mathcal{V}_{\beta q}^* \langle C_{\alpha k \bar{\sigma}}^\dagger C_{\beta q \bar{\sigma}} \rangle + \Sigma_0 \langle C_{\alpha k \bar{\sigma}}^\dagger d_{\bar{\sigma}} \rangle) \right], \quad (33)$$

$$\Sigma_2 = \Sigma_3 - \Sigma_1, \quad (34)$$

$$\Sigma_3 = \sum_{\alpha k} \left[\frac{|\mathcal{V}_{\alpha k}|^2}{\omega - \varepsilon_{\alpha k}} + \frac{|\mathcal{V}_{\alpha k}|^2}{\omega + \varepsilon_{\alpha k} - 2\varepsilon_d - U} \right], \quad (35)$$

$$\langle \tilde{n}_{\bar{\sigma}} \rangle = \langle n_{\bar{\sigma}} \rangle + \sum_{\alpha k} \frac{\mathcal{V}_{\alpha k}^*}{\omega - \varepsilon_{\alpha k}} \langle d_{\bar{\sigma}}^\dagger C_{\alpha k \bar{\sigma}} \rangle + \sum_{\alpha k} \frac{\mathcal{V}_{\alpha k}}{\omega_1 - \varepsilon_{\alpha k}} \langle C_{\alpha k \bar{\sigma}}^\dagger d_{\bar{\sigma}} \rangle, \quad (36)$$

with $\omega_1 = -\omega + 2\varepsilon_d + U$. Here, Σ_0 is the tunneling self-energy which in the wide-band limit is approximated as $\Sigma_0 \approx \Lambda(\omega) - i\Gamma$ where $\Lambda(\omega)$ is the principal value of Σ_0 . Σ_i ($i = 1, 2, 3$) are additional self-energies which depend on the expectation values $\langle d_{\bar{\sigma}}^\dagger C_{\alpha k \bar{\sigma}} \rangle$ and $\langle C_{\beta q \bar{\sigma}}^\dagger C_{\alpha k \bar{\sigma}} \rangle$. In Ref. [81], Meir *et al.* assume $\langle C_{\beta q \bar{\sigma}}^\dagger C_{\alpha k \bar{\sigma}} \rangle \approx f_\alpha(\omega) \delta_{\alpha\beta} \delta_{kq} \delta_{\sigma s}$ and $\langle d_{\bar{\sigma}}^\dagger C_{\alpha k \bar{\sigma}} \rangle \approx 0$. Nevertheless, in general the expectation values are functions of the lesser Green's function $G^<$ that should be calculated with the help of a modified fluctuation-dissipation theorem [77] to account for the nonequilib-

rium situation

$$\langle A^\dagger B \rangle = -\frac{1}{2\pi i} \int d\omega \mathcal{F}(\omega) (\langle B, A^\dagger \rangle^r - \langle B, A^\dagger \rangle^a), \quad (37)$$

where the function $\mathcal{F}(\omega)$ is the effective non-equilibrium distribution function of the system [Eq. (19)] and $\langle B, A^\dagger \rangle^{r,a}$ is the Fourier transform of the retarded (advanced) correlator $\langle B(t), A^\dagger(t') \rangle^{r,a} = -\frac{i}{\hbar} \theta(t \mp t') \langle [A^\dagger(t'), B(t)]_+ \rangle$, A and B being two arbitrary second-quantization operators. Finally, Eq. (36) depends on the occupation of the quantum dot $\langle n_{\bar{\sigma}} \rangle$ and is calculated self-consistently from

$$\langle n_{\sigma} \rangle = \frac{1}{2\pi i} \int d\omega G_{\sigma,\sigma}^<(\omega). \quad (38)$$

Employing Eq. (37), we write the lesser dot Green function as $G_{\sigma,\sigma}^<(\omega) = -2i\mathcal{F}(\omega)\text{Im}[G_{\sigma,\sigma}^r(\omega)]$.

A. Infinite Coulomb interaction

When U is very large ($U \rightarrow \infty$), we immediately see that both Σ_2 and Σ_3 drop from Eq. (31). Therefore, the dot Green's function reads

$$G_{\sigma,\sigma}^r(\omega) = \frac{1 - \langle \tilde{n}_{\bar{\sigma}} \rangle}{\omega - \varepsilon_d - \Sigma_0 - \Sigma_1}, \quad (39)$$

with

$$\Sigma_1 = \sum_{\alpha k} \frac{\mathcal{V}_{\alpha k}^*}{\omega - \varepsilon_{\alpha k}} \left[\sum_{\beta q} (\mathcal{V}_{\beta q} \langle C_{\beta q \bar{\sigma}}^\dagger C_{\alpha k \bar{\sigma}} \rangle - \Sigma_0 \langle d_{\bar{\sigma}}^\dagger C_{\alpha k \bar{\sigma}} \rangle) \right], \quad (40)$$

$$\langle \tilde{n}_{\bar{\sigma}} \rangle = \langle n_{\bar{\sigma}} \rangle + \sum_{\alpha k} \frac{\mathcal{V}_{\alpha k}^*}{\omega - \varepsilon_{\alpha k}} \langle d_{\bar{\sigma}}^\dagger C_{\alpha k \bar{\sigma}} \rangle, \quad (41)$$

The expectation values $\langle C_{\beta q \bar{\sigma}}^\dagger C_{\alpha k \bar{\sigma}} \rangle$ and $\langle d_{\bar{\sigma}}^\dagger C_{\alpha k \bar{\sigma}} \rangle$ in Eq. (40) and (41) are evaluated using Eq. (37). We next follow Ref. 82, which discusses a decoupling scheme for solving the set of EOM. By doing this, Eqs. (40) and (41) respectively become

$$\Sigma_1(\omega) = -\frac{i\Gamma}{2} + \mathcal{X}(\omega)[1 + 2i\Gamma G_{\bar{\sigma},\bar{\sigma}}^a(\omega)]\Gamma, \quad (42)$$

$$\langle \tilde{n}_{\bar{\sigma}} \rangle = \langle n_{\bar{\sigma}} \rangle + \Gamma G_{\bar{\sigma},\bar{\sigma}}^a(\omega) \mathcal{X}(\omega), \quad (43)$$

where $\mathcal{X}(\omega) = \sum_{\alpha} \Gamma_{\alpha} X_{\alpha}(\omega)/\Gamma$ and X_{α} is defined as

$$\begin{aligned} X_{\alpha}(\omega) &= \int_{-D}^D \frac{d\omega'}{\pi} \frac{f_{\alpha}(\omega') - 1/2}{\omega - \omega' + i0^+} \\ &= \frac{1}{\pi} \left[\frac{1}{2} \ln \frac{D^2 - \omega^2}{(2\pi k_B T_{\alpha})^2} - \psi \left(\frac{1}{2} - \frac{i(\omega - \mu_{\alpha})}{2\pi k_B T_{\alpha}} \right) \right] \end{aligned} \quad (44)$$

Due to the digamma function, Eq. (44) contains logarithmic divergences that are responsible for the emergence of the Kondo singularity. Finally, the QD retarded Green's function takes the form

$$G_{\sigma,\sigma}^r(\omega) = g(\omega) \left[\delta n_{\sigma} + \frac{iQ(\omega)}{\mathcal{X}^*(\omega)} \right], \quad (45)$$

with

$$z = \frac{\omega - \varepsilon_d - \Lambda(\omega)}{2\Gamma}, \quad (46)$$

$$g(\omega) = \frac{1}{\omega - \varepsilon_d - \delta\varepsilon_d + i3\Gamma/2}, \quad (47)$$

$$Q(\omega) = S(\omega) - \sqrt{S^2(\omega) + |\mathcal{X}(\omega)|^2 \left(\frac{3}{2} \delta n_{\sigma} - \delta n_{\sigma}^2 \right)}, \quad (48)$$

$$S(\omega) = z^2 + \frac{9}{16} - z\text{Re}[\mathcal{X}(\omega)] + \left(\delta n_{\sigma} - \frac{3}{4} \right) \text{Im}[\mathcal{X}(\omega)] \quad (49)$$

where $\delta n_{\sigma} = 1 - \langle n_{\sigma} \rangle$. Equation (45) has two different terms. The first term in the right-hand side depends only on δn_{σ} and is responsible for the dot mean-field resonance. The second term is responsible for the Kondo singularity that becomes prominent for $T < T_K$. Equation (45) depends on the occupation given by Eq. (38).

Once we have determined the retarded dot Green's function, we can analyze the behavior of the local density of states. First, we estimate the Kondo temperature from Haldane's formula [72]

$$T_K = \sqrt{D\Gamma} e^{-\pi|\varepsilon_d|/2\Gamma}. \quad (50)$$

As expected, a Kondo peak is visible in the spectral function $\rho_d(\omega) = \sum_{\sigma} \rho_{d\sigma}(\omega)$ defined as

$$\rho_{d\sigma} = -\frac{1}{\pi} \text{Im}[G_{\sigma,\sigma}^r(\omega)]. \quad (51)$$

This narrow resonance will survive as long as $T < T_K$ and, by increasing T , smears out until it completely disappears [82].

The impact of voltage and temperature biases on the spectral function is illustrated in Fig. 9. First, for the voltage-driven case the Kondo resonance becomes split with resonances $\omega \approx \pm eV/2$ [Fig. 9(a)], as experimentally observed [10]. Yet, the employed EOM scheme does not capture the dephasing effect generated by the voltage shift. A combination of EOM using the dot occupation computed with the non-crossing approximation has been proposed to amend the lack of dephasing when a voltage is considered [11, 77, 83]. For the temperature-driven case, we recall out thermal configuration in which only the left contact is heated, $T_L = T + \theta$, whereas the right reservoir is kept at the background temperature, $T_R = T$. Our results are depicted in Fig. 9(b). As expected, the main effect of the thermal gradient is to smear out the Kondo singularity. However, a further increase of the temperature difference does not cause the Kondo peak to vanish even for $\theta \gg T_K$ [see Fig. 9(b)]. This can be understood as follows. The Kondo resonance in EOM arises from the sharp character of the Fermi function. In this case, even though one of the Fermi functions becomes sufficiently smooth as θ increases, the other contact Fermi function remains sharp for a low background temperature. As a consequence, even if θ grows considerably the Kondo peak is never totally quenched. This behavior is an artifact of the EOM approach since it does

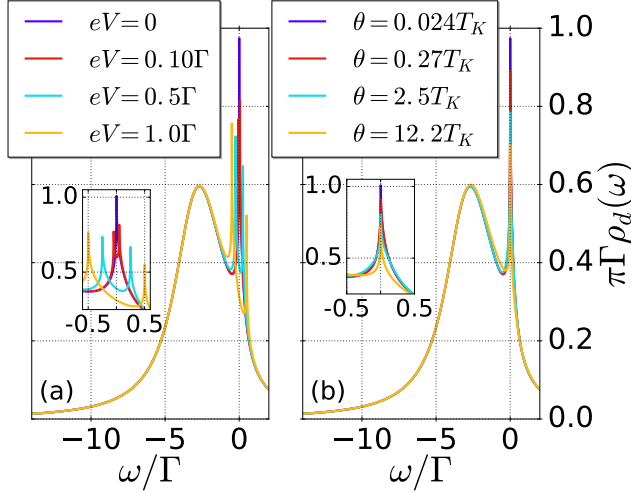


FIG. 9. (Color online). (a) Nonequilibrium infinite- U quantum dot spectral density of states for different eV values. Inset: Detail of the density of states around the Fermi energy ($\varepsilon_F = 0$). (b) Nonequilibrium infinite- U quantum dot spectral density of states for different thermal gradients. The background temperature is set at $T = 0.024T_K$. Inset: Detail of the density of states around the Fermi energy ($\varepsilon_F = 0$). Parameters: $\varepsilon_d = -3.5\Gamma$, $D = 100\Gamma$, $T = 0.024T_K$.

not account for dephasing processes as we earlier pointed out. However, this method gives the correct behavior at low θ : a thermal bias does not split the Kondo resonance but gradually destroys the peak, in agreement with the perturbative approach and the mean-field slave-boson theory.

B. Finite Coulomb interaction

In this section, we generalize our previous findings to the case where the Coulomb interaction is finite. In this case, Eqs. (33), (35) and (36) take the following forms

$$\Sigma_1 = -i\Gamma + \Gamma\mathcal{X}(\omega)[1 + 2i\Gamma G_{\bar{\sigma},\bar{\sigma}}^a(\omega)] - \Gamma\mathcal{X}^*(\omega_1)[1 + 2i\Gamma G_{\bar{\sigma},\bar{\sigma}}^r(\omega_1)], \quad (52)$$

$$\Sigma_3 = \delta\varepsilon_d(\omega) + \delta\varepsilon_d(\omega_1) - 2i\Gamma, \quad (53)$$

$$\langle \tilde{n}_{\bar{\sigma}} \rangle = \langle n_{\bar{\sigma}} \rangle + \Gamma[G_{\bar{\sigma},\bar{\sigma}}^a(\omega)\mathcal{X}(\omega) - G_{\bar{\sigma},\bar{\sigma}}^r(\omega_1)\mathcal{X}(\omega_1)]. \quad (54)$$

Note that now the retarded Green's function depends recursively on itself, which makes the decoupling scheme a highly nontrivial task. In order to make further progress we consider a finite but large U interaction. Hence, we can safely neglect $G^r(\omega_1)$ and find an explicit expression for the following retarded Green's function

$$G_{\sigma,\sigma}^r(\omega) = g_u(\omega) \left[\delta n_u + \frac{iQ_u(\omega)}{\mathcal{X}_u^*(\omega)} \right], \quad (55)$$

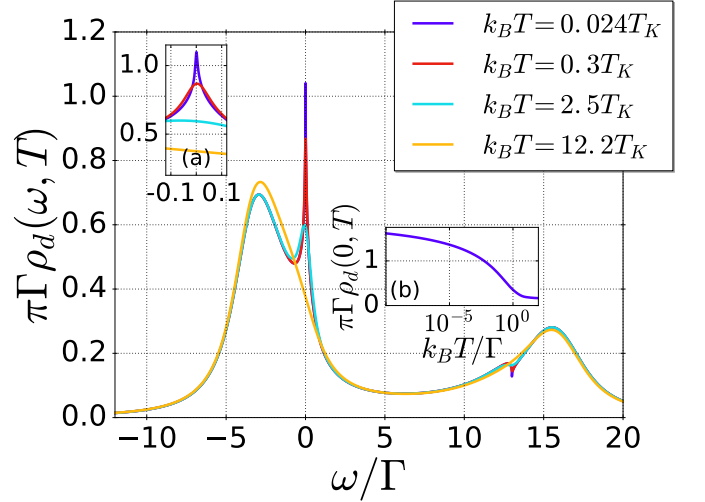


FIG. 10. (Color online). Finite- U quantum dot spectral density at equilibrium background temperatures. Parameters: $\varepsilon_d = -3.5\Gamma$, $D = 100\Gamma$, $U = 20\Gamma$. Insets: (a) Blow up of the dot spectral density of states around the Fermi energy. (b) Height of the Kondo peak as a function of the background temperature.

Here the quantities entering in Eq. (55) depend on the function $u(\omega) = U/(\Sigma_0 + \Sigma_3 + \varepsilon_d + U - \omega)$:

$$\mathcal{X}_u(\omega) = u(\omega)\mathcal{X}(\omega), \quad (56)$$

$$g_u(\omega) = \frac{1}{2\Gamma(z + i(1+u)/2 + \bar{\mathcal{X}}_u)}, \quad (57)$$

$$Q_u(\omega) = S_u - (S_u^2 - |\mathcal{X}_u^* \delta n_u|^2 + |\mathcal{X}_u|^2 [\delta n_u h_1(\omega) - 2\text{Im}[\delta n_u] h_2(\omega)])^{1/2}, \quad (58)$$

$$S_u(\omega) = z^2 + \frac{|1+u|^2}{4} - \frac{\text{Im}[\bar{\mathcal{X}}_u(1+u)]}{2} + \frac{|\bar{\mathcal{X}}_u|^2}{4} - z\text{Re}[\mathcal{X}_u] - \frac{\text{Im}[\mathcal{X}_u(1+u^*)]}{2} - \frac{\text{Re}[\mathcal{X}_u \bar{\mathcal{X}}_u]}{2} + \text{Im}[\mathcal{X}_u \delta n_u^*] - z\text{Im}[u] + z\text{Re}[\bar{\mathcal{X}}_u], \quad (59)$$

where the bar indicates that the function is to be computed as $\bar{f} \equiv f(\omega_1)$. In Eq. (58) we have defined the functions $h_1(\omega) = -\text{Im}[\mathcal{X}_u] + 1 + \text{Re}[u]$, $h_2(\omega) = z + i(1+u)/2 + \bar{\mathcal{X}}_u/2$ and $\delta n_u = 1 - u(\omega)\langle n_{\sigma} \rangle$. Figure 10 shows our results for the dot spectral density [Eq. (51)] at high background temperatures. As expected, the dot DOS consists of two mean-field resonances, one centered at $\omega = \varepsilon_d$ and another at $\omega = \varepsilon_d + U$ and the Kondo singularity at $\omega \approx 0$. For these results we take into account a modified Kondo temperature for a system with finite U [1]

$$T_K \approx \sqrt{2\Gamma U} \exp \left\{ -\frac{\pi|\varepsilon_d|(U + \varepsilon_d)}{2\Gamma U} \right\}. \quad (60)$$

We observe in Fig. 10 that the Kondo peak is quenched as long as the background temperature surpasses the Kondo temperature, as expected. Additionally, the inset of Fig. 10 shows the amplitude of the Kondo peak

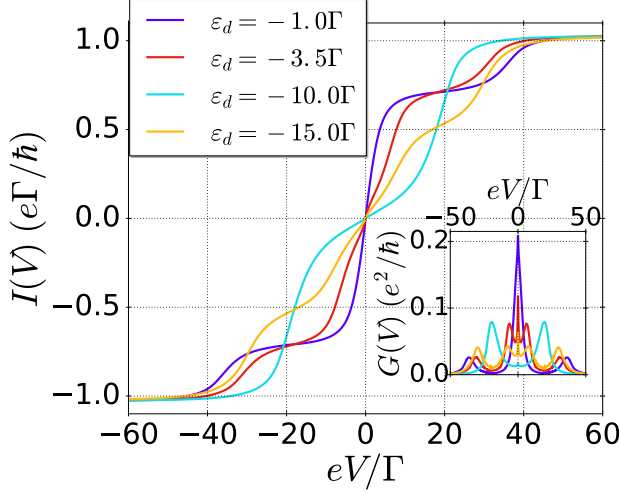


FIG. 11. (Color online). I - V characteristics at different dot level positions. Inset: Differential electric conductance vs voltage bias for the given values of the energy level. Parameters: $D = 100\Gamma$, $k_B T = 0.0001\Gamma$, $U = 20\Gamma$, and $\Gamma_L = \Gamma_R = \Gamma/2$.

as a function of T . This results confirms the fact that a high temperature destroys the Kondo singularity as long as $T > T_K$ even when we consider finite charging energies. We have also extended our study of the dot DOS for finite U to the nonequilibrium case by considering the influence of a voltage and temperature gradient. We observe qualitatively similar results (not shown here) as those obtained for the infinite U case [Fig. 9]. We find that given voltage leads to a Kondo peak splitting whereas a temperature gradient smears out the Kondo singularity.

C. Voltage-driven transport

We proceed to the transport properties of the system. We calculate the current from Eq. (28) using Eq. (55). The integrals over energy of the self-consistent calculation are now solved numerically. Figure 11 shows the I - V characteristic for different dot gate positions. The data display a staircase-like behavior where the step transitions take place whenever the bias voltage aligns with the dot resonances. By direct differentiation, we find the differential conductance curves shown in the inset of Fig. 11. Here, when $\varepsilon_d < -\Gamma$ we find five different peaks, four located when the mean field resonances aligns with the electrochemical potential of the leads [$eV \approx \pm 2\varepsilon_d$ and $eV \approx \pm 2(\varepsilon_d + U)$] and the Kondo zero bias anomaly centered at equilibrium ($V = 0$). Whenever a resonance occurs the I - V has a visible jump. Our calculation is performed at finite temperature. Therefore, the Kondo peak is apparent in the differential conductance only for sufficiently negative dot gate positions.

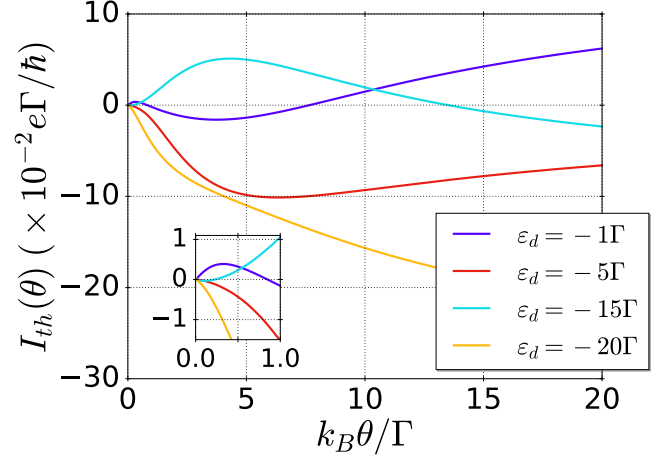


FIG. 12. (Color online). Thermocurrent versus the thermal gradient for different dot gate positions. Inset: Detail of the thermocurrent at low thermal gradients. Parameters: $U = 20\Gamma$, $D = 100\Gamma$, $k_B T = 0.01\Gamma$, and $\Gamma_L = \Gamma_R = \Gamma/2$.

D. Temperature-driven transport

We consider now the thermoelectric response of the electrical current in Fig. 12. The thermocurrent is calculated for the thermal configuration sketched in Fig. 1. Depending on the energy level ε_d we find different regions where the thermocurrent behaves distinctively: if $\varepsilon_d > 0$ or $\varepsilon_d + U < 0$ we find that the dot resonances are either above (empty orbital regime) or below (full orbital regime) the Fermi energy. Then, for these dot gate positions the thermocurrent either decreases or increases monotonously (e.g., in Fig. 12 for $\varepsilon_d = -20\Gamma$). Otherwise, when $0 > \varepsilon_d > -U$ the $I_{th}(\theta)$ curves change sign. Remarkably, the nontrivial zeros occur at different energy scales determined by either spin fluctuations ($k_B T_K$) or charge fluctuations (U): see, e.g., the case $\varepsilon_d = -\Gamma$ with a nontrivial zero at around $k_B \theta = \Gamma$ and another zero at around $k_B \theta = 10\Gamma$. Notice that for very negative dot gate positions the nontrivial zero of the thermoelectric current associated with the Kondo scale may not occur due to the fact that for those level values the Kondo temperature is exceedingly small and one has $T > T_K$.

When we calculate the differential thermoelectric conductance, we recover the butterfly structure (not shown here) reported previously for the Coulomb blockade regime in Ref. 34. Such singular pattern is a direct consequence of the presence of the two mean-field resonances lying at $\varepsilon_d = 0$ and $\varepsilon_d = -U$. Thus, in Fig. 13, we show the three resonances located approximately at $\omega \approx \varepsilon_d$, $\omega \approx \varepsilon_d + U$, and the Kondo peak at $\omega = \varepsilon_F = 0$. In the very low temperature regime the only open transport channel is due to the Kondo singularity in which electrons flow from one lead to another. Away from the particle-hole symmetry point, the Kondo peak becomes

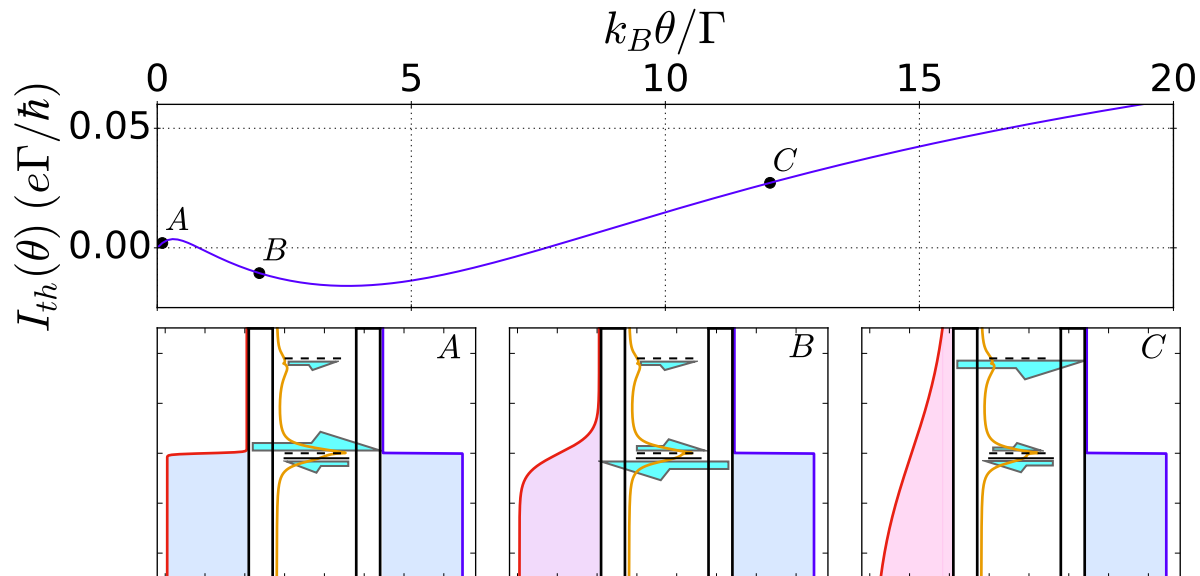


FIG. 13. (Color online). Top: Thermocurrent versus θ for $\varepsilon_d = -\Gamma$ as taken from Fig. 12. Bottom: Energy diagram corresponding to the current states marked in the upper panel. Red (blue) line indicates the Fermi-Dirac function of the left (right) reservoir where orange curve corresponds to the spectral function for the three points (A, B and C) indicated in the top panel. ε_d is indicated with a black line. Dashed lines corresponds to the $\varepsilon_F = 0$ and $\varepsilon_d + U$ energies. Finally, the arrows show the direction and intensity of the electronic flow through the corresponding resonance.

asymmetric. Then, if we heat the left reservoir, electrons tend to flow from the left to right side (case A of Fig. 13). Increasing θ , the mean field resonance at ε_d starts to contribute to the current flow but in the opposite direction and eventually it dominates over the Kondo resonance. In between (case B), for a given value of θ the current vanishes. Further increasing of θ opens the higher mean-field resonance at $\varepsilon_d + U$, which favors electron tunneling from left to right, i.e., opposite to the previous current flow. As a consequence, an additional sign change of the thermoelectrical current takes place (case C).

VI. CONCLUSIONS

In closing, we have examined the nonequilibrium thermoelectric effects of a correlated quantum dot connected to two electronic reservoirs. We have employed different theoretical approximations with different ranges of validity. As a first attempt, we have applied the perturbative analysis to the Kondo Hamiltonian when a thermal and a voltage bias is present. Interestingly, we find that the Kondo temperature decreases monotonically in the presence of a thermal gradient when one reservoir is heated. At very low temperatures, we have employed the infinite- U slave-boson mean-field theory suitable for the Fermi liquid regime. Here, we obtain a very good agreement with the perturbative results for the behavior of T_K

when a thermal shift is considered. Finally, in order to investigate the density of states in the high and moderate temperature regime we have applied the equation-of-motion scheme to our setup. By using this approach we are able to capture both Coulomb blockade and Kondo physics. We consider both infinite and finite charging energies. We observe that the Kondo peak splits under the action of a voltage bias. In the case of a thermal gradient, the Kondo peak decreases slowly. Finally, we have analyzed both the $I - V$ characteristic and the thermoelectric current. For the latter we find the existence of nontrivial zeros at two distinct energy scales ($k_B\theta$), each associated with Kondo correlations and charge fluctuations. We explain the existence of these nontrivial zeros due to a change of the flow caused by the contribution of the different resonances as long as θ grows. We believe that an experimental test of our theoretical predictions is within the reach of present transport techniques.

VII. ACKNOWLEDGMENTS

We thank R. Aguado for useful discussions. This work has been supported by MINECO under Grants FIS2014-52564, CAIB and FEDER.

Appendix A: Calculation of the conductance

The goal of this appendix is to find an expression for the electrical conductance using the expectation value of Eq. (8). We start our calculation performing a perturbation expansion around the coupling constant $\mathcal{J}_{\alpha\beta}^{(0)}$ (see Ref. [71]). To first order in perturbation theory, the electrical current is absent $\langle \hat{I}(0) \rangle = 0$. Therefore, we need to start at second order where the current, after some algebraic manipulations, takes the form

$$I^{(2)} = \left(-\frac{2}{\hbar}\right) \sum_{\alpha\beta} \mathcal{J}_{\alpha\beta}^{(0)} \text{Im} \left[\int_{-\infty}^0 dt e^{-\frac{i\epsilon}{\hbar}(V_\alpha - V_\beta)t} \times \langle \bar{T}[x_{\sigma s} C_{\tilde{\alpha}}^\dagger C_{\tilde{\beta}} \hat{I}(0)] \rangle \right], \quad (\text{A1})$$

where \bar{T} is the anti-time-ordering operator. To make the notation more compact, we have defined in Eq. (A1) the sets $\tilde{\alpha} \equiv \{\alpha, k, \sigma\}$ and $\tilde{\beta} \equiv \{\beta, q, s\}$. Inserting Eq. (10) into Eq. (A1) and applying Wick's theorem to the expectation

values, the electrical current turns out to be

$$I^{(2)} = -2e \left[\mathcal{J}_{LR}^{(0)} \right]^2 \left(\sum_{\sigma_1 \sigma_2} \langle \bar{T}[x_{\sigma_1 \sigma_2} x_{\sigma_2 \sigma_1}] \rangle \right) \sum_{\alpha} (1 - 2\delta_{\alpha R}) \times \int_{-\infty}^0 dt \text{Re} \left[\sum_{k_1 k_2} e^{-\frac{i\epsilon}{\hbar}(V_\alpha - V_{\tilde{\alpha}})t} g_{\alpha k_1}^{\bar{t}}(0, t) g_{\tilde{\alpha} k_2}^{\bar{t}}(0, t) \right], \quad (\text{A2})$$

where $g_{\alpha k_1}^{\bar{t}}(t_1, t_2)$ is the anti-time-ordered Green's function of the free electrons in lead α . It reads

$$g_{\alpha k_1}^{\bar{t}}(t_1, t_2) = -\frac{i}{\hbar} e^{-\frac{i}{\hbar} \epsilon_{\alpha k_1} (t_1 - t_2)} [\theta(t_2 - t_1) - f_\alpha(\epsilon_{\alpha k_1})]. \quad (\text{A3})$$

Using the identity $\sum_{\sigma_1 \sigma_2} \langle \bar{T}[x_{\sigma_1 \sigma_2} x_{\sigma_2 \sigma_1}] \rangle = 1/2$, substituting Eq. (A3) into Eq. (A2) and solving the integral in time and in k_i , we find

$$I^{(2)} = -\frac{e^2 \pi}{\hbar} \nu^2 \left[\mathcal{J}_{LR}^{(0)} \right]^2 V. \quad (\text{A4})$$

Therefore, the second-order conductance term becomes constant independently of temperature. Hence, we need to compute the third order in perturbation theory:

$$I^{(3)} = -\frac{1}{\hbar^2} \sum_{\tilde{\alpha}_i \tilde{\beta}_i} \mathcal{J}_{\alpha_1 \beta_1}^{(0)} \mathcal{J}_{\alpha_2 \beta_2}^{(0)} \text{Re} \left[\int_{-\infty}^0 dt_2 \int_{-\infty}^0 dt_1 e^{-\frac{i\epsilon}{\hbar}(V_{\alpha_1} - V_{\beta_1})t_1} e^{-\frac{i\epsilon}{\hbar}(V_{\alpha_2} - V_{\beta_2})t_2} \langle \bar{T}[x_{\sigma_1 s_1} C_{\tilde{\alpha}_1}^\dagger C_{\tilde{\beta}_1} x_{\sigma_2 s_2} C_{\tilde{\alpha}_2}^\dagger C_{\tilde{\beta}_2} \hat{I}(0)] \rangle \right] + \frac{1}{\hbar^2} \sum_{\tilde{\alpha}_i \tilde{\beta}_i} \mathcal{J}_{\alpha_1 \beta_1}^{(0)} \mathcal{J}_{\alpha_2 \beta_2}^{(0)} \text{Re} \left[\int_{-\infty}^0 dt_2 \int_{-\infty}^0 dt_1 e^{-\frac{i\epsilon}{\hbar}(V_{\alpha_1} - V_{\beta_1})t_1} e^{-\frac{i\epsilon}{\hbar}(V_{\alpha_2} - V_{\beta_2})t_2} \langle x_{\sigma_1 s_1} C_{\tilde{\alpha}_1}^\dagger C_{\tilde{\beta}_1} \hat{I}(0) x_{\sigma_2 s_2} C_{\tilde{\alpha}_2}^\dagger C_{\tilde{\beta}_2} \rangle \right]. \quad (\text{A5})$$

Now, we separate both terms in the right hand side of Eq. (A5) as $I^{(3a)}$ and $I^{(3b)}$. We proceed in the same way

as the second order and apply Wick's theorem. After lengthy but straightforward algebra, we find

$$I^{(3a)} = e \sum_{\alpha\beta} \left[\mathcal{J}_{LR}^{(0)} \right]^2 \mathcal{J}_{\alpha\alpha}^{(0)} \left(\sum_{\sigma_i} \langle \bar{T}[x_{\sigma_1 \sigma_2}(t_1) x_{\sigma_2 \sigma_3}(t_2) x_{\sigma_3 \sigma_1}(0)] \rangle + \langle \bar{T}[x_{\sigma_1 \sigma_2}(t_2) x_{\sigma_3 \sigma_1}(t_1) x_{\sigma_2 \sigma_3}(0)] \rangle \right) (1 - 2\delta_{\beta L}) \times \int_{-\infty}^0 dt_1 \int_{-\infty}^0 dt_2 \text{Re} \left[\sum_{k_i} e^{-\frac{i\epsilon}{\hbar}(V_\beta - V_\alpha)t_1} e^{-\frac{i\epsilon}{\hbar}(V_\alpha - V_\beta)t_2} g_{\beta k_1}^{\bar{t}}(0, t_1) g_{\alpha k_2}^{\bar{t}}(t_1, t_2) g_{\tilde{\beta} k_3}^{\bar{t}}(t_2, 0) \right], \quad (\text{A6})$$

$$I^{(3b)} = -e \sum_{\alpha\beta} \left[\mathcal{J}_{LR}^{(0)} \right]^2 \mathcal{J}_{\alpha\alpha}^{(0)} \left(\sum_{\sigma_i} \langle x_{\sigma_1 \sigma_2} x_{\sigma_2 \sigma_3} x_{\sigma_3 \sigma_1} \rangle \right) \int_{-\infty}^0 dt_1 \int_{-\infty}^0 dt_2 (1 - 2\delta_{\beta L}) \text{Re} \left[\sum_{\{k_i\}} e^{-\frac{i\epsilon}{\hbar}(V_\alpha - V_\beta)t_1} e^{-\frac{i\epsilon}{\hbar}(V_\beta - V_\alpha)t_2} \times g_{\beta k_1}^>(0, t_2) g_{\alpha k_2}^<(t_2, t_1) g_{\tilde{\beta} k_3}^>(t_1, 0) \right] - e \sum_{\alpha\beta} \left[\mathcal{J}_{LR}^{(0)} \right]^2 \mathcal{J}_{\alpha\alpha}^{(0)} \left(\sum_{\sigma_i} \langle x_{\sigma_1 \sigma_2} x_{\sigma_3 \sigma_1} x_{\sigma_2 \sigma_3} \rangle \right) \times \int_{-\infty}^0 dt_1 \int_{-\infty}^0 dt_2 (1 - 2\delta_{\beta R}) \text{Re} \left[\sum_{k_i} e^{-\frac{i\epsilon}{\hbar}(V_\beta - V_\alpha)t_1} e^{-\frac{i\epsilon}{\hbar}(V_\alpha - V_\beta)t_2} g_{\beta k_1}^<(0, t_1) g_{\alpha k_2}^>(t_1, t_2) g_{\tilde{\beta} k_3}^<(t_2, 0) \right], \quad (\text{A7})$$

where $g_{\alpha k}^<$ and $g_{\alpha k}^>$ are the lesser and greater Green's function for electrons on lead α . The spin expectation

values of Eq. (A6) depends on the time ordering and yield $5/8 + (3/8)\text{sgn}(t_2 - t_1)$, with $\text{sgn}(t)$ the sign function.

Meanwhile, the terms in Eq. (A7) are independent of time and the spin expectation values are thus 1/8 and 1/2, respectively. Substituting these values and the definition of the Green's function in Eq. (A3),

$$g_{\alpha k \sigma}^<(t_1, t_2) = \frac{i}{\hbar} e^{-\frac{i}{\hbar} \varepsilon_{\alpha k \sigma} (t_1 - t_2)} f_{\alpha}(\varepsilon_{\alpha k \sigma}), \quad (\text{A8})$$

$$g_{\alpha k \sigma}^>(t_1, t_2) = -\frac{i}{\hbar} e^{-\frac{i}{\hbar} \varepsilon_{\alpha k \sigma} (t_1 - t_2)} (1 - f_{\alpha}(\varepsilon_{\alpha k \sigma})), \quad (\text{A9})$$

$$\begin{aligned} I^{(3)} = & \frac{e}{8\hbar^3} \sum_{\alpha\beta} \left[\mathcal{J}_{LR}^{(0)} \right]^2 \mathcal{J}_{\alpha\alpha}^{(0)} (1 - 2\delta_{\beta L}) \int_{-\infty}^0 dt_1 \int_{-\infty}^0 dt_2 \{ (5 - 3\text{sgn}(t_2 - t_1)) \\ & \times \text{Im} \left[\sum_{k_i} e^{-\frac{i}{\hbar} [\varepsilon_{\alpha k_2} - \varepsilon_{\beta k_1} + e(V_{\beta} - V_{\alpha})] t_1} e^{-\frac{i}{\hbar} [\varepsilon_{\beta k_3} - \varepsilon_{\alpha k_2} + e(V_{\alpha} - V_{\beta})] t_2} f_{\beta}(\varepsilon_{\beta k_1}) (\theta(t_2 - t_1) - f_{\alpha}(\varepsilon_{\alpha k_2})) (1 - f_{\beta}(\varepsilon_{\beta k_3})) \right] \\ & - \text{Im} \left[\sum_{k_i} e^{-\frac{i}{\hbar} [\varepsilon_{\alpha k_2} - \varepsilon_{\beta k_1} + e(V_{\beta} - V_{\alpha})] t_1} e^{-\frac{i}{\hbar} [\varepsilon_{\beta k_3} - \varepsilon_{\alpha k_2} + e(V_{\alpha} - V_{\beta})] t_2} (f_{\alpha}(\varepsilon_{\alpha k_2}) - f_{\beta}(\varepsilon_{\beta k_1}) f_{\alpha}(\varepsilon_{\alpha k_2}) - f_{\beta}(\varepsilon_{\beta k_3}) f_{\alpha}(\varepsilon_{\alpha k_2}) \right. \\ & \left. - 4f_{\beta}(\varepsilon_{\beta k_3}) f_{\beta}(\varepsilon_{\beta k_1}) + 5f_{\beta}(\varepsilon_{\beta k_3}) f_{\alpha}(\varepsilon_{\alpha k_2}) f_{\beta}(\varepsilon_{\beta k_1})) \right] \}. \end{aligned} \quad (\text{A10})$$

We next combine the Fermi functions of Eq. (A10) and perform the sums over the wavenumbers k_i by transforming them into integrals. We solve the resulting integrals by performing the Fourier transform of the Fermi function:

$$\int_{-\infty}^{\infty} d\omega \frac{e^{-i\omega t}}{1 + e^{\hbar\omega/k_B T}} = \frac{\pi i}{\sinh \frac{\pi k_B T}{\hbar}}. \quad (\text{A11})$$

$$\begin{aligned} I^{(3)} = & -\frac{e\pi^3}{8\hbar^2} \nu^3 \left[\mathcal{J}_{LR}^{(0)} \right]^2 \sum_{\alpha\beta} \mathcal{J}_{\alpha\alpha}^{(0)} (1 - 2\delta_{\beta L}) \int_{-\infty}^0 dt \left[3\text{Bs}_{\beta\bar{\beta}}(t) - \text{Bs}_{\beta\alpha}(t) + \text{Bs}_{\alpha\bar{\beta}}(t) \right] \\ & - \frac{e\pi^3}{8\hbar^2} \nu^3 \left[\mathcal{J}_{LR}^{(0)} \right]^2 \sum_{\alpha\beta} \mathcal{J}_{\alpha\alpha}^{(0)} (1 - 2\delta_{\beta L}) \text{Re} \left[\int_{-\infty}^0 dt_2 e^{-\frac{i\varepsilon}{\hbar} (V_{\alpha} - V_{\beta}) t_2} \int_{-\infty}^0 dt_1 e^{-\frac{i\varepsilon}{\hbar} (V_{\beta} - V_{\alpha}) t_1} \text{Ts}_{\beta\alpha\bar{\beta}}(t_1, t_2) \right], \end{aligned} \quad (\text{A12})$$

where we define the functions

$$\text{Bs}_{\alpha\gamma}(t) = \frac{\sin[e(V_{\alpha} - V_{\gamma})t/\hbar]}{\beta_{\alpha}\beta_{\gamma} \sinh \frac{\pi t}{\beta_{\alpha}\hbar} \sinh \frac{\pi t}{\beta_{\gamma}\hbar}}, \quad (\text{A13})$$

$$\text{Ts}_{\alpha\gamma\delta}(t_1, t_2) = \frac{\text{sgn}(t_2 - t_1)}{\beta_{\alpha}\beta_{\gamma}\beta_{\delta} \sinh \frac{\pi t_1}{\beta_{\alpha}\hbar} \sinh \frac{\pi(t_1 - t_2)}{\beta_{\gamma}\hbar} \sinh \frac{\pi t_2}{\beta_{\delta}\hbar}}, \quad (\text{A14})$$

with $\beta_{\alpha} = 1/k_B T_{\alpha}$ the inverse temperature of lead α . Finally, after solving the sum over α and β we obtain

$$\begin{aligned} I^{(3)} = & \frac{3e\pi^3}{4\hbar^2} \nu^3 \left[\mathcal{J}_{LR}^{(0)} \right]^2 \left(\mathcal{J}_{LL}^{(0)} + \mathcal{J}_{RR}^{(0)} \right) \\ & \times \int_{-\infty}^0 dt \frac{\sin(eVt/\hbar)}{\beta_L\beta_R \sinh \frac{\pi t}{\beta_L\hbar} \sinh \frac{\pi t}{\beta_R\hbar}}. \end{aligned} \quad (\text{A15})$$

Once we have the third order term, we are interested in the linear conductance $G = \partial I / \partial V|_{V=0}$, which defines

the current up to the third order reads

Then, the current becomes

the height of the Kondo resonance. Applying the voltage derivative to Eq. (A4) and Eq. (A15) the conductance is given by

$$\begin{aligned} G = & -\frac{e^2\pi}{\hbar} \nu^2 \left[\mathcal{J}_{LR}^{(0)} \right]^2 + \frac{3e^2\pi^3}{4\hbar^3} \nu^3 \left[\mathcal{J}_{LR}^{(0)} \right]^2 \left(\mathcal{J}_{LL}^{(0)} + \mathcal{J}_{RR}^{(0)} \right) \\ & \times \int_{-\infty}^0 dt \frac{t}{\beta_L\beta_R \sinh \frac{\pi t}{\beta_L\hbar} \sinh \frac{\pi t}{\beta_R\hbar} + D_0^{-2}}. \end{aligned} \quad (\text{A16})$$

We note that we have added the energy bandwidth $D_0 = \sqrt{-\varepsilon_d(U + \varepsilon_d)}$ to the integral in order to find a convergent solution. Additionally, we need to assume that the minimum time of the integral in Eq. (A16) is related to the temperatures as $\tau \approx \hbar\sqrt{\beta_L\beta_R}$. These assumptions yield Eq. (11).

Appendix B: Equation of motion beyond Hartree-Fock

The aim of this appendix is to give more details of the equation-of-motion calculation yielding Eq. (31). Firstly, we compute the equation of motion for the re-

tarded Green's function

$$(i\hbar\partial_t - \varepsilon_d)G_{\sigma,\sigma}^r(t, t') = \delta(t-t') + \sum_{\alpha k} \mathcal{V}_{\alpha k} G_{\alpha k \sigma, \sigma}^r + U \langle\langle d_\sigma n_{\bar{\sigma}}, d_\sigma^\dagger \rangle\rangle. \quad (\text{B1})$$

Equation (B1) depends on $\langle\langle d_\sigma n_{\bar{\sigma}}, d_\sigma^\dagger \rangle\rangle$, which is a higher order correlator. Considering that $U \gg k_B T, \Gamma$ we calculate the equation of motion for $\langle\langle d_\sigma n_{\bar{\sigma}}, d_\sigma^\dagger \rangle\rangle$,

$$(i\hbar\partial_t - \varepsilon_d - U) \langle\langle d_\sigma n_{\bar{\sigma}}, d_\sigma^\dagger \rangle\rangle = \langle n_{\bar{\sigma}} \rangle \delta(t-t') + \sum_{\alpha k} \mathcal{V}_{\alpha k}^* [\langle\langle C_{\alpha k \sigma} n_{\bar{\sigma}}, d_\sigma^\dagger \rangle\rangle + \langle\langle d_\sigma d_\sigma^\dagger C_{\alpha k \bar{\sigma}}, d_\sigma^\dagger \rangle\rangle] - \sum_{\alpha k} \mathcal{V}_{\alpha k} \langle\langle d_\sigma C_{\alpha k \bar{\sigma}}^\dagger d_\sigma, d_\sigma^\dagger \rangle\rangle. \quad (\text{B2})$$

At this point, if we determine the EOM of $\langle\langle C_{\alpha k \sigma} n_{\bar{\sigma}}, d_\sigma^\dagger \rangle\rangle$ and neglect the contributions of the correlators $\langle\langle d_\sigma d_\sigma^\dagger C_{\alpha k \bar{\sigma}}, d_\sigma^\dagger \rangle\rangle$, $\langle\langle d_\sigma C_{\alpha k \bar{\sigma}}^\dagger d_\sigma, d_\sigma^\dagger \rangle\rangle$, $\langle\langle C_{\alpha k \sigma} C_{\beta q \bar{\sigma}}^\dagger d_\sigma, d_\sigma^\dagger \rangle\rangle$ and $\langle\langle C_{\alpha k \sigma} d_\sigma^\dagger C_{\beta q \bar{\sigma}}, d_\sigma^\dagger \rangle\rangle$ we arrive at the two peak solu-

tion that has been widely investigated [84]. However, our interest for the moment is to take a step further and include Kondo correlations. We follow the calculation of Lacroix [85] and Kashcheyevs *et al.* [86] and extend the EOM scheme by computing the evolution of these higher order correlators

$$(i\hbar\partial_t - \varepsilon_{\alpha k}) \langle\langle C_{\alpha k \sigma} n_{\bar{\sigma}}, d_\sigma^\dagger \rangle\rangle = \mathcal{V}_{\alpha k} \langle\langle d_\sigma n_{\bar{\sigma}}, d_\sigma^\dagger \rangle\rangle + \sum_{\beta q} [\mathcal{V}_{\beta q}^* \langle\langle C_{\alpha k \sigma} d_\sigma^\dagger C_{\beta q \bar{\sigma}}, d_\sigma^\dagger \rangle\rangle - \mathcal{V}_{\beta q} \langle\langle C_{\alpha k \sigma} C_{\beta q \bar{\sigma}}^\dagger d_\sigma, d_\sigma^\dagger \rangle\rangle], \quad (\text{B3})$$

$$(i\hbar\partial_t - \varepsilon_{\alpha k}) \langle\langle d_\sigma d_\sigma^\dagger C_{\alpha k \bar{\sigma}}, d_\sigma^\dagger \rangle\rangle = \langle d_\sigma^\dagger C_{\alpha k \bar{\sigma}} \rangle \delta(t-t') + \mathcal{V}_{\alpha k} \langle\langle d_\sigma n_{\bar{\sigma}}, d_\sigma^\dagger \rangle\rangle + \sum_{\beta q} [\mathcal{V}_{\beta q}^* \langle\langle C_{\beta q \sigma} d_\sigma^\dagger C_{\alpha k \bar{\sigma}}, d_\sigma^\dagger \rangle\rangle - \mathcal{V}_{\beta q} \langle\langle d_\sigma C_{\beta q \bar{\sigma}}^\dagger C_{\alpha k \bar{\sigma}}, d_\sigma^\dagger \rangle\rangle], \quad (\text{B4})$$

$$(i\hbar\partial_t + \delta\varepsilon_{\alpha k}) \langle\langle d_\sigma C_{\alpha k \bar{\sigma}}^\dagger d_\sigma, d_\sigma^\dagger \rangle\rangle = \langle C_{\alpha k \bar{\sigma}}^\dagger d_\sigma \rangle \delta(t-t') - \mathcal{V}_{\alpha k}^* \langle\langle d_\sigma n_{\bar{\sigma}}, d_\sigma^\dagger \rangle\rangle + \sum_{\beta q} \mathcal{V}_{\beta q} [\langle\langle C_{\beta q \sigma} C_{\alpha k \bar{\sigma}}^\dagger d_\sigma, d_\sigma^\dagger \rangle\rangle + \langle\langle d_\sigma C_{\alpha k \bar{\sigma}}^\dagger C_{\beta q \bar{\sigma}}, d_\sigma^\dagger \rangle\rangle], \quad (\text{B5})$$

where $\delta\varepsilon_{\alpha k} = \varepsilon_{\alpha k} - 2\varepsilon_d - U$. New higher order correlators are generated in the process. Then, in order to obtain a solvable system of differential equations, we consider the

approximation proposed by Mattis [86, 87]

$$\langle\langle A^\dagger BC, D^\dagger \rangle\rangle \approx \langle A^\dagger B \rangle \langle\langle C, D^\dagger \rangle\rangle - \langle A^\dagger C \rangle \langle\langle B, D^\dagger \rangle\rangle. \quad (\text{B6})$$

Therefore, after applying Eq. (B6) to Eqs. (B3), (B4) and (B5) the system of equations can be closed. In the Fourier space, we end up with Eq. (31).

-
- [1] See, e. g., A. C. Hewson, *The Kondo problem to Heavy Fermions* (Cambridge University Press, Cambridge, 1993).
 - [2] D. Goldhaber-Gordon, H. Shtrikman, D. Mahalu, D. Abusch-Magder, U. Meirav and M. A. Kastner, *Nature* (London) **391**, 156 (1998).
 - [3] S. M. Cronenwett, T. H. Oosterkamp and L. P. Kouwenhoven, *Science* **281**, 540 (1998).
 - [4] J. Schmid, J. Weis, K. Eberl and K. v. Klitzing, *Physica B* **256-258**, 182 (1998).
 - [5] S. Sasaki, S. De Franceschi, J. M. Elzerman, W. G. van der Wiel, M. Eto, S. Tarucha and L. P. Kouwenhoven, *Nature* (London) **405**, 764 (2000).

-
- [6] W. G. van der Wiel, S. De Franceschi, T. Fujisawa, J. M. Elzerman, S. Tarucha and L. P. Kouwenhoven, *Science* **289**, 2105 (2000).
 - [7] T. K. Ng and P. A. Lee, *Phys. Rev. Lett.* **61**, 1768 (1988).
 - [8] L. I. Glazman and M. E. Raikh, *JETP Lett.* **47**, 452 (1988).
 - [9] T. A. Costi, A. C. Hewson and V. Zlatic, *J. Phys. Condens. Matter* **6**, 2519 (1994).
 - [10] S. De Franceschi, R. Hanson, W. G. van der Wiel, J. M. Elzerman, J. J. Wijkema, T. Fujisawa, S. Tarucha, and L. P. Kouwenhoven, *Phys. Rev. Lett.* **89**, 156801 (2002).
 - [11] A. Rosch, J. Kroha and P. Wölfle, *Phys. Rev. Lett.* **87**, 156802 (2001).

- [12] R. Aguado and D. C. Langreth, Phys. Rev. Lett. **85**, 1946 (2000).
- [13] R. Zitko, J. Bronca, A. Ramsak, and T. Rejec, Phys. Rev. B **73**, 153307 (2006).
- [14] J. Martinek, M. Sindel, L. Borda, J. Barnaś, J. König, G. Schön, and J. von Delft, Phys. Rev. Lett. **91**, 247202 (2003).
- [15] M. S. Choi, D. Sánchez, and R. López, Phys. Rev. Lett. **92**, 056601 (2003).
- [16] J. C. Cuevas, A. Levy Yeyati, and A. Martín-Rodero, Phys. Rev. B **63**, 094515 (2001).
- [17] Q.-f. Sun, H. Guo, and T.-h. Lin, Phys. Rev. Lett. **87**, 176601 (2001).
- [18] D. Sánchez and R. López, Phys. Rev. B **71**, 035315 (2005).
- [19] T. L. Schmidt, A. Komnik, and A. O. Gogolin, Phys. Rev. Lett. **98**, 056603 (2007).
- [20] *Thermoelectrics Handbook. Macro to Nano*, edited by D.M. Rowe (CRC Press, Boca Raton, FL, 2006).
- [21] R. Venkatasubramanian, E. Siivola, T. Colpitts, and B. O'Quinn, Nature **413**, 597 (2001).
- [22] L. W. Molenkamp, H. van Houten, C. W. J. Beenakker, R. Eppenga, and C. T. Foxon, Phys. Rev. Lett. **65**, 1052 (1990).
- [23] A. S. Dzurak, C. G. Smith, C. H. W. Barnes, M. Pepper, L. Martín-Moreno, C. T. Liang, D. A. Ritchie, and G. A. C. Jones, Phys. Rev. B **55**, R10197 (1997).
- [24] P. Reddy, S.-Y. Jang, R. A. Segalman, and A. Majumdar, Science **315**, 1568 (2007).
- [25] J.-H. Jiang, O. Entin-Wohlman, and Y. Imry, Phys. Rev. B **85**, 075412 (2012).
- [26] Y. M. Zuev, W. Chang, and P. Kim, Phys. Rev. Lett. **102**, 096807 (2009).
- [27] P. Wei, W. Bao, Y. Pu, C. Ning Lau, and J. Shi, Phys. Rev. Lett. **102**, 166808 (2009).
- [28] R. Sánchez, B. Sothmann, and A. N. Jordan, Phys. Rev. Lett. **114**, 146801 (2015).
- [29] L. Vannucci, F. Ronetti, G. Dolcetto, M. Carrega, and M. Sassetti, Phys. Rev. B **92**, 075446 (2015).
- [30] R. Takahashi and S. Murakami, Phys. Rev. B **81**, 161302(R) (2010).
- [31] S.-Y. Hwang, R. López, M. Lee, and D. Sánchez, Phys. Rev. B **90**, 115301 (2014).
- [32] A. A. M. Staring, L. W. Molenkamp, B. W. Alphenaar, H. van Houten, O. J. A. Buyk, M. A. A. Mabe-soone, C. W. J. Beenakker, and C. T. Foxon, Europhys. Lett. **22**, 57 (1993).
- [33] S. F. Svensson, E. A. Hoffmann, N. Nakpathomkun, P. M. Wu, H. Q. Xu, H.A. Nilsson, D. Sánchez, V. Kashcheyevs and H. Linke, New J. Phys. **15**, 105011 (2013).
- [34] M. A. Sierra and D. Sánchez, Phys. Rev. B **90**, 115313 (2014).
- [35] A. Svilans, A. M. Bunke, S. F. Svensson, M. Leijnse and H. Linke, Physica E **82**, 34 (2016).
- [36] D. Sánchez and R. López, arXiv:1604.00855 (C. R. Physique, in press, 2016).
- [37] D. Boese and R. Fazio, Europhys. Lett. **56** (4), 576 (2001).
- [38] B. Dong and X. L. Lei, J. Phys. Condens. Matter **14**, 11747 (2002).
- [39] M. Krawiec and K. I. Wysokinski, Phys. Rev. B, **75**, 155330 (2007).
- [40] J. Azema, A.-M. Daré, S. Schäfer and P. Lombardo, Phys. Rev. B **86**, 075303 (2012).
- [41] N. A. Zimbovskaya, J. Chem. Phys. **142**, 244310 (2015).
- [42] P. Dutt and K. L. Hur, Phys. Rev. B **88**, 235133 (2013).
- [43] A. Dorda, M. Ganahl, S. Andergassen, W. von der Linden, and E. Arrigoni, arXiv:1608.05714 (preprint, 2016).
- [44] S. Kirchner, F. Zamani, E. Muñoz, *Nonlinear thermoelectric response of quantum dots: Renormalized dual fermions out of equilibrium*, in *New Materials for Thermoelectric Applications: Theory and Experiment* (V. Zlatic and A. Hewson, eds.), pp. 129–168 (Springer, 2012).
- [45] R. Scheibner, H. Buhmann, D. Reuter, M. N. Kiselev, and L. W. Molenkamp, Phys. Rev. Lett. **95**, 176602 (2005).
- [46] T. A. Costi and V. Zlatic, Phys. Rev. B **81**, 235127 (2010).
- [47] J. Zhou and R. Yang, Phys. Rev. B **82**, 075324 (2010).
- [48] T.-S. Kim and S. Hershfield, Phys. Rev. B **67**, 165313 (2003).
- [49] M. Krawiec and K. Wysokiński, Phys. Rev. B **73**, 075307 (2006).
- [50] I. Weymann and J. Barnaś, Phys. Rev. B **88**, 085313 (2013).
- [51] S. Andergassen, T. A. Costi, and V. Zlatic, Phys. Rev. B **84**, 241107(R) (2011).
- [52] T. Rejec, R. Zitko, J. Mravlje, and A. Ramsak, Phys. Rev. B **85**, 085117 (2012).
- [53] R. Zitko, J. Mravlje, A. Ramsak, and T. Rejec, New J. Phys. **15**, 105023 (2013).
- [54] P. S. Cornaglia, G. Usaj, and C. A. Balseiro, Phys. Rev. B **86**, 041107 (2012).
- [55] P. Roura-Bas, L. Tosi, A. A. Aligia, and P. S. Cornaglia, Phys. Rev. B **86**, 165106 (2012).
- [56] N. A. Zimbovskaya, J. Chem. Phys. **140**, 104706 (2014).
- [57] L. Karwacki, P. Trocha, and J. Barnaś, J. Phys.: Condens. Matter **25**, 505305 (2013).
- [58] D. M. Kennes and V. Meden, Phys. Rev. B **87**, 075130 (2013).
- [59] J. S. Lim, R. López, and D. Sánchez, New J. Phys. **16**, 015003 (2014).
- [60] L. Ye, D. Hou, R. Wang, D. Cao, X. Zheng, and Y. Yan, Phys. Rev. B **90**, 165116 (2014).
- [61] R. Chirla and C. P. Moca, Phys. Rev. B **89**, 045132 (2014).
- [62] K. P. Wójcik and I. Weymann, Phys. Rev. B **89**, 165303 (2014).
- [63] S. B. Tooski, A. Ramsak, B. R. Bulka, and R. Zitko, New J. Phys. **16**, 055001 (2014).
- [64] S. Donsa, S. Andergassen, and K. Held, Phys. Rev. B **89**, 125103 (2014).
- [65] K. P. Wójcik and I. Weymann, Phys. Rev. B **93**, 085428 (2016).
- [66] P. W. Anderson, Phys. Rev. **124**, 41 (1961).
- [67] M. Pustilnik, Y. Avishai, and K. Kikoin, Phys. Rev. Lett. **84**, 1756 (2000).
- [68] J. Paaske, A. Andersen, and K. Flensberg, Phys. Rev. B **82**, 081309(R) (2010).
- [69] M. Pletyukhov and D. Schuricht, Phys. Rev. B **84**, 041309(R) (2011).
- [70] A. Kaminski, Y. V. Nazarov and L. I. Glazman, Phys. Rev. Lett. **83**, 384 (1999).
- [71] A. Kaminski, Y. V. Nazarov, and L. I. Glazman, Phys. Rev. B **62**, 8154 (2000).
- [72] F. D. M. Haldane, Phys. Rev. Lett. **40**, 416 (1978).

- [73] A. C. Hewson, Phys. Rev. Lett. **70**, 4007 (1993).
- [74] A. Oguri and A. Hewson, J. Phys. Soc. Japan **74**, 988 (2005).
- [75] P. Coleman, Phys. Rev. B **29**, 3035 (1984).
- [76] See, e.g., H. Haug and A.-P. Jauho, *Quantum Kinetics in Transport and Optics of Semiconductors* (Springer, Berlin, 2007).
- [77] C. A. Balseiro, G. Usaj, and M. J. Sánchez, J. Phys.: Condens. Matter **22**, 425602 (2010).
- [78] P. Coleman, C. Hooley, Y. Avishai, Y. Goldin, and A. F. Ho, J. Phys.: Condens. Matter **14**, 205 (2002).
- [79] R. López, R. Aguado, and G. Platero, Phys. Rev. B **69**, 235305 (2004).
- [80] M. Wagner, Phys. Rev. B **44**, 6104 (1991).
- [81] Y. Meir and N. S. Wingreen, Phys. Rev. Lett. **68**, 2512, (1992).
- [82] O. Entin-Wohlman, A. Aharony and Y. Meir, Phys. Rev. B **71**, 035333 (2005).
- [83] Y. Meir, N. S. Wingreen, and P. A. Lee, Phys. Rev. Lett. **70**, 2601 (1993).
- [84] A. C. Hewson, Phys. Rev. **144**, 420 (1966).
- [85] C. Lacroix, J. Phys. F: Metal Physics **11**, 2389 (1981).
- [86] V. Kashcheyevs, A. Aharony, O. Entin-Wohlman, Phys. Rev. B **73**, 125338 (2006).
- [87] A. Theumann, Phys. Rev. **178**, 978 (1969).